AGU100 ADVANCING EARTH AND SPACE SCIENCE

JGR

Journal of Geophysical Research: Earth Surface

RESEARCH ARTICLE
10.1029/2017JF004431

**Key Points:**
- An advective-diffusive formulation of incision/alluviation in bedrock-alluvial rivers captures morphodynamics of a periodic *sedimentograph*
- Steady state longitudinal profile shows upstream boundary layer *pocket* accommodating thick (up to tens of meters), transient alluvial deposits
- Steady state bedrock longitudinal profile takes a universal form: profile for a short reach is a truncated version of that of a longer reach

**Supporting Information:**
- Supporting Information S1
- Data Set S1
- Data Set S2

**Correspondence to:**
L. Zhang,
lizhangpig@gmail.com

**Citation:**
Zhang, L., Stark, C., Schumer, R., Kwang, J., Li, T., Fu, X., et al. (2018). The advective-diffusive morphodynamics of mixed bedrock-alluvial rivers subjected to spatiotemporally varying sediment supply. *Journal of Geophysical Research: Earth Surface, 123*, 1731–1755. https://doi.org/10.1029/2017JF004431

Received 14 JUL 2017
Accepted 24 JUN 2018
Accepted article online 23 JUL 2018
Published online 13 AUG 2018



# The Advective-Diffusive Morphodynamics of Mixed Bedrock-Alluvial Rivers Subjected to Spatiotemporally Varying Sediment Supply

**Li Zhang[1,2,3], Colin Stark[4], Rina Schumer[3], Jeffrey Kwang[5], Tiejian Li[1,2], Xudong Fu[1], Guangqian Wang[1,2], and Gary Parker[5,6]**

[1]State Key Laboratory of Hydroscience and Engineering, Tsinghua University, Beijing, China, [2]School of Water Resources and Electric Power, Qinghai University, Xining, China, [3]Division of Hydrologic Sciences, Desert Research Institute, Reno, NV, USA, [4]Lamont-Doherty Earth Observatory of Columbia, University Palisades, Palisades, NY, USA, [5]Department of Civil and Environmental Engineering, University of Illinois Urbana-Champaign, Urbana, IL, USA, [6]Department of Geology, University of Illinois Urbana-Champaign, Urbana, IL, USA

**Abstract** Mountain rivers subject to earthquakes and intense precipitation have highly variable sediment supply rates. Here we consider the morphodynamics of 1-D mixed bedrock-alluvial rivers with temporally varying sediment supply rates. We use a periodic sedimentograph, characterized by short periods of high sediment feed rate and longer periods of low sediment feed rate. We study the problem with a corrected Macroroughness Saltation-Abrasion-Alluviation model. In this model, incision is driven by bedload colliding with bedrock, but incision can be turned off by either zero sediment transport or complete alluviation. The formulation is advective-diffusive, the former capturing upstream-migrating knickpoints and the latter capturing smearing of the sedimentograph downstream. The steady state balance between incision and uplift is characterized by a bedrock slope that varies downstream, exhibiting low values at the upstream end of the domain and higher values farther downstream. Sufficiently far downstream, the bedrock slope approaches that predicted for constant feed rates. The zone of low slope near the feed point corresponds to a *pocket* (zone of locally depressed bedrock slope) in the longitudinal profile, which is repeatedly drowned in and flushed of sediment. The steady state slope profile of a shorter reach is a truncated version of that of a longer reach. A limiting reach length including the pocket defines a sedimentograph boundary layer, where the effects of sediment feed fluctuation are felt.

## 1. Introduction

Mountain landscapes are sculpted by a myriad of processes acting over a wide range of spatiotemporal scales (e.g., Whipple, 2004). Aside from glaciers, rivers provide the main conduits for delivering sediment from the hillslopes to sinks such as lakes, the ocean, or adjacent plains. Sediment supply to rivers may be gradual, as in the case of delivery by overland flow, or episodic, in the form of landslides or debris flows. This sediment is ultimately transported out of the system by fluvial processes. In the case of landscapes undergoing relative uplift, the rivers that transport sediment delivered from hillslopes are generally mixed bedrock-alluvial streams, with only partial alluvial cover. This partial cover allows the river to incise in response to tectonic uplift or a drop in external base level. The interaction between sediment supply, transport, and incision under the constraint of set downstream base level change, according to which the bedrock can be alternately exposed or covered to varying degrees, determines the evolution toward a long-term balance between rock uplift and bedrock incision (Zhang et al., 2015). But how should this balance be established?

In mountainous regions, the assumption of constant sediment supply is not generally valid. Instead, the system must accommodate repeated episodic sediment delivery from, for example, landslides, followed by removal (e.g., Yanites et al., 2010). Streams that receive their sediment from landslides have a dual supply and sediment transport control on sediment load, such that they may not transport significant amounts of sediment unless it is provided by landsliding (e.g., Attal, 2017; Benda & Dunne, 1997; Golly et al., 2017; Hovius et al., 2000).


**Figure 1.** (a) View of the Tangjiashan landslide dam formed by the 2008 Wenchuan earthquake, Sichuan, China. The coordinates for this landslide are (31°50′45.6″N, 104°27′36″E). Channel width upstream of the landslide dam is ~ 50 m. Image is courtesy of Xinhua News Agency (Zhu Wei). (http://archive.boston.com/bigpicture/2008/05/after_the_quake.html). (b) Landslide at Taiyuan South Creek, Taidong, eastern Taiwan (24°56′46.54″N, 121°13′44.72″E). The width and length of this landslide are 100 and 270 m approximately. The photograph was taken in 2016. The bedrock is mudstone. The image is courtesy of Ching-Fang Lee and Hsien-Ter Chou. (c) Landslide at Xiayuan Creek, Taoyuan, northwest Taiwan (24°48′21.32″N, 121°22′18.90″E). The width and length of this landslide are 20 and 52 m approximately. The photograph was taken in 2016. The bedrock is interbedded shale sandstone. The image is courtesy of Ching-Fang Lee and Hsien-Ter Chou.

The aftermath of individual episodic sediment supply events to mountain rivers, whether natural or caused by, for example, hydraulic mining, has been studied by Lisle et al. (1997), Ferguson et al. (2015), and Croissant et al. (2017). Lisle et al. (1997, 2001), Cui, Parker, Lisle et al. (2003), Cui, Parker, Pizzuto et al. (2003), Sklar et al. (2009), and Venditti et al. (2010) have performed experimental and numerical studies of the evolution of alluvial pulses in mountain rivers. Lisle et al. (2001) and Cui, Parker, Lisle et al. (2003) have shown that as long as the bed remains covered with alluvium, the response to massive alluviation is a gradual diffusion of the initial pulse pile. In none of these cases was the role of exposed or partially exposed bedrock considered. Such a condition may arise as the sediment pile is depleted.

Zhang et al. (2015) have shown that in streams underlain by bedrock, as long as the alluvial cover is incomplete, waves of alluvium can propagate downstream. They have shown that the interplay between advection and diffusion of alluvium dictates how punctuated sediment supply is exported from the system. This interplay also influences the way in which incision, and thus the stream profile, evolves in response to uplift. One way to address the issue of river response to punctuated sediment supply is through distributed landscape evolution models that specifically incorporate factors such as bedrock incision, alluvial cover, stochasticity in sediment supply, and hydrology (e.g., Egholm et al., 2013; Gasparini et al., 2007; Lague, 2010). Here we consider a simpler reach-based approach, based on the previous work of Zhang et al. (2015).

Our single river reach has length $L$. Sediment is supplied to the reach at the upstream end in the form of a repeated sedimentograph, so as to approximate both the episodic effects of landslides and more gradual delivery processes associated with overland flow. A sedimentograph is the analog of a hydrograph, except that it is sediment load rather than discharge that varies in time (An, Cui, et al., 2017; Zhang et al., 2015). The river has a bedrock base but may be either partially or fully alluviated at any given time.

The central goal of this paper is the study of the morphodynamic response of both alluvial cover and bedrock incision to the repeated introduction of sediment pulses generated by this sedimentograph. We study both transient evolution toward and the manifestation of the macroscopic steady state balance between rock uplift and incision associated with repeated sedimentographs.

Inspired by Hovius et al. (2000), our sedimentographs consist of a (short) period of relatively high sediment input followed by a (long) period of relatively low sediment input. The periods of relatively high sediment input are meant to mimic supply from landslides. Landslides can cause short-term river aggradation as high as 20 m (Huang & Montgomery, 2012) and can expose bedrock as much as 30-m deep (Chou et al., 2017). Landslides in tectonically active areas (Sichuan and Taiwan, China) adjacent to mixed bedrock-alluvial streams are illustrated in Figure 1.

Herein we specifically model neither landslide dynamics nor the short-term morphodynamics of the breaching of landslide dams. Instead, we model the medium-term morphodynamics of the piles of sediment emplaced in channels by landslides and the long-term morphodynamics of incision of the bedrock surface underlying the alluvium.


**Figure 2.** View of the mixed bedrock-alluvial Shimanto River, Shikoku, Japan. (a) View of the river itself, which has a width of ~ 100 m. (b) View of local bed with gravel alluvium and bedrock outcrops. The calculations presented herein are based on conditions for the Shimanto River but are expected to be applicable to a wider range of mixed bedrock-alluvial channels.

Our formulation for bedrock incision consists of a slightly corrected version of the Macroroughness Saltation-Abrasion-Alluviation (MRSAA) model of Zhang et al. (2015), which is in turn a descendant of the Capacity Saltation Abrasion (CSA) model of Sklar and Dietrich (2004, 2006). Bedrock incision is accomplished by abrasion as clasts collide with the bedrock surface. The essential difference between the two is that MRSAA captures bedrock and alluvial morphodynamics simultaneously, allowing for periodically complete alluviation as sediment from a landslide overwhelms the bedrock surface and allowing for the downstream transmission of damped sediment waves over bedrock. The essential elements of the model are illustrated in Figure 2, which shows a reach of the Shimanto River in Japan. As explained in Zhang et al. (2015), the Shimanto River is an archetypal and quantifiable example of a mixed bedrock-alluvial river that shows substantial bedrock exposure at low flow. The bedrock itself is seen to have some characteristic roughness (macroroughness); alluvium must completely inundate the roughness elements in order for the channel to become completely alluviated.

Our paper is structured as follows. In section 2, we quantify the sedimentograph in terms of a high upstream supply rate, a low upstream supply rate, and a duration for each. We can increase the sedimentograph peakedness, and thus its episodicity, by increasing the high-supply rate or by decreasing the duration over which it is maintained. The corrected MRSAA (MRSAA-c) model for incisional-alluvial morphodynamics is introduced in section 3. This model specifically computes the interplay between advection and diffusion of alluvium, and also allows for periods of complete alluviation, when the bedrock is buried in sediment and bedrock incision is turned off. Simulation conditions and input parameters are specified in section 4. Section 5 provides a comprehensive analysis of the effect of the upstream sedimentograph in determining both alluvial and incisional morphodynamics as a macroscopic steady state balance between rock uplift and incision is achieved. We specifically address the issues of (a) the role of peakedness of the sedimentograph in setting alluvial/incisional morphodynamics, (b) the role of diffusion in damping advective waves of sediment, thus limiting the length of the reach influenced by the sedimentograph, (c) the influence of the sedimentograph on the steady state bedrock longitudinal profile, (d) the pattern of sediment aggradation and evacuation during one cycle at steady state, and (e) the role of stochasticity in sediment supply. We present our discussion in section 6 and conclusions in section 7 separately.

## 2. Channel Configuration and Quantification of Temporally Varying Sediment Supply

The highly simplified configuration we consider here is the same as that described in Zhang et al. (2015). We omit many features of mountain rivers so that we can focus as much as possible on the effect of temporally varying sediment supply. Our river reach is 1-D with constant width $B$. For each run, water discharge is held constant at a flood value $Q$ for fraction of time $I$ (flood intermittency); flood waves are not modeled. Sediment is gravel moving as bedload, and only a single size $D$ is considered. All sediment is fed in at the upstream end; there are no tributaries to supply either water or sediment. Grain size diminution due to abrasion or

comminution is not considered. The stream is subject to rock uplift at the spatiotemporally constant rate $\upsilon$. The elevation variation of the bedrock surface is characterized in terms of a macroroughness $L_{mr}$. The only mechanism for bedrock incision considered is wear due to gravel clasts colliding with the bedrock.

The relaxation of these conditions is relatively straightforward. For example, Parker (1991a, 1991b) has considered grain diminution by abrasion; Lague et al. (2005) and DiBiase and Whipple (2011) have characterized water discharge variation in terms of a probability density function; Chatanantavet and Parker (2009) have considered incision due to plucking; Chatanantavet et al. (2010) have considered downstream fining of coarse sediment with side input; and An, Fu, et al. (2017) have considered both sediment mixtures and unsteady flow in mountain rivers. We do not consider these features here because our goal is the first-order modeling of the effect of a repeated sedimentograph on mixed bedrock-alluvial morphodynamics.

Here we study numerically the time evolution of the profile of a river reach of length $L$ as it approaches a steady state balance between incision and uplift. Our analysis is not intended for the modeling of specific events but rather for long-term evolution. This long-term evolution can, however, be established by repeated episodic inputs of sediment that can completely bury the bedrock surface of a river in alluvium, so turning off bedrock incision for some period of time. We inquire as to how repeated burial and exposure of bedrock affects the evolution of the bedrock profile itself, as well as its alluvial cover. In this regard, Yanites et al. (2010) note that "landslides induced by the earthquake [that is, the 1999 $M_w$ = 7.6 Chi-Chi earthquake in central Taiwan] mantle bedrock on the river bed with sediment, impeding incision for decades to centuries as the material is evacuated", whereas Hancox et al. (2005) document the removal of 50–60% of a landslide dam over 4 years.

Our model is a slight variation on the one given in Zhang et al. (2015); more details are given in section 3. We first introduce our quantification of cyclically varying sediment supply in terms of a feed *sedimentograph* applied at the upstream end of the reach.

The feed sedimentograph is defined in terms of a period $T$, including a time of high feed $T_h$ and a time of low feed $T_l$ such that $T = T_h + T_l$. The mean feed rate per unit width $q_{af,m}$ over the sedimentograph represents the average of a high feed rate per unit width $q_{af,h}$ for time $T_h$, followed by a low feed rate per unit width $q_{af,l}$ for time $T_l$. These feed rates correspond to flood events. The river is assumed to be in flood for fraction (flood intermittency) $I$ of the time. We define

$$r_h = \frac{T_h}{T}, \quad r_l = \frac{T_l}{T} \tag{1a}$$

so that by definition,

$$r_l = 1 - r_h \tag{1b}$$

and

$$q_{af,h} r_h + q_{af,l} r_l = q_{af,m}. \tag{2}$$

We define the ratios for sediment feed as follows:

$$r_{qh} = \frac{q_{af,h}}{q_{af,m}}, r_{ql} = \frac{q_{af,l}}{q_{af,m}}. \tag{3}$$

It is found from equations (1a) to (3) that

$$r_{ql} = \frac{1 - r_{qh} r_h}{1 - r_h}. \tag{4}$$

Figure 3 illustrates two sample sedimentographs. In these samples, we use the mean feed rate $q_{af,m}$ = 0.000834 $m^2/s$ specified in Table 1 and derived from Zhang et al. (2015), where $q_{af}$ denotes the volume sediment feed rate per unit channel width, and a period $T$ = 40 years. Using parameters specified in Table 1, that is, flood intermittency $I$ = 0.05, channel width $B$ = 100 m, and sediment submerged specific gravity $R$ = 1.65, this corresponds to an annual rate of 3.5 × $10^5$ t/year in the calculational examples presented

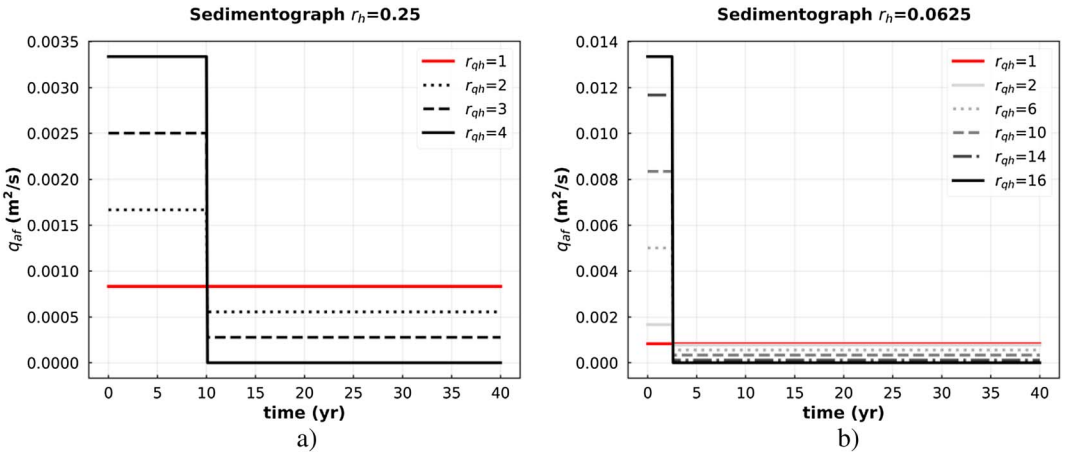


**Figure 3.** (a) Feed sedimentograph for the case $T$ = 40 years, $q_{af,m}$ = 0.000834 m$^2$/s (3.5 × 10$^5$ t/year), and $r_h$ = 0.25. The ratio $r_{qh}$ of high feed rate to mean feed rate varies from 1 (constant feed rate) to the maximum value of 4. (b) Feed sedimentograph for the case $T$ = 40 years, $q_{af,m}$ = 0.000834 m$^2$/s (3.5 × 10$^5$ t/year), and $r_h$ = 0.0625. The ratio $r_{qh}$ of high feed rate to mean feed rate varies from 1 (constant feed rate) to the maximum value of 16.

below. We consider two values for the duration of the high feed period, that is, $T_h$ = 10 years and $T_h$ = 2.5 years, corresponding to $r_h$ = 0.25 and $r_h$ = 0.0625 (as shown in Table 1). The resulting sedimentographs are shown in Figure 3a for the case $r_h$ = 0.25, in which case $r_{qh}$, that is, the ratio of the high feed rate to the mean feed rate, ranges from 1 (constant feed) to 4 (feed rate is 4 times the mean feed rate for time $T_h$ and is zero for time $T_l$). The case $r_h$ = 0.0625, in which case $r_{qh}$ ranges from 1 (constant feed) to 16 (feed rate is 16 times the mean feed rate for time $T_h$ and is 0 for time $T_l$), is shown in Figure 3b.

The sedimentographs given in Figure 3 are intended to be generic examples. In a more site-specific analysis, the work of Larsen et al. (2010) and Marc et al. (2016), for example, can be used to tie the sedimentograph specifically to landslide volume or volume of a series of landslides driving the period of high alluvial feed.

**Table 1**
*Model Inputs*

| Parameter | Definition | Value (s) | Notes |
|---|---|---|---|
| $Q$ | Flood discharge | 300 m$^3$/s | Morphodynamically active discharge |
| $I$ | Flood intermittency | 0.05 | Fraction of time when the river is morphodynamically active: former value used when bedrock morphodynamics is considered |
| $B$ | Channel width | 100 m | |
| $D$ | Sediment grain size | 20 mm | |
| $R$ | Submerged specific gravity of sediment | 1.65 | |
| $Cz$ | Dimensionless Chezy resistance coefficient | 10 | |
| $\lambda$ | Alluvial porosity | 0.35 | |
| $L_{mr}$ | Thickness of macroroughness layer | 1 m | |
| $L$ | Reach length | 20 km | Base value: other values considered |
| $\beta$ | Wear coefficient | 0.05 km$^{-1}$ | |
| $\upsilon$ | Uplift rate | 5.0 mm/year | |
| $S_b$, $S_{bi}$ | Bedrock slope | 0.004 | Initial value $S_{bi}$; one other value of $S_{bi}$ (0.0015) is also considered |
| $q_{af,m}$ | Mean bedload feed rate averaged over sedimentograph | 0.000834 m$^2$/s | This sediment feed rate corresponds to an annual volume rate of 1.3 × 10$^5$ m$^3$/year and an annual mass feed rate of 3.5 × 10$^5$ t/year. The approximate equivalent catchment-scale averaged erosion rate is 0.325 mm/year for the Shimanto River basin, which has an area of around 400 km$^2$ |
| $T$ | Period of sedimentograph | 40 years | |
| $T_h$ | Duration of high feed rate of sedimentograph | 2.5 or 10 years | |

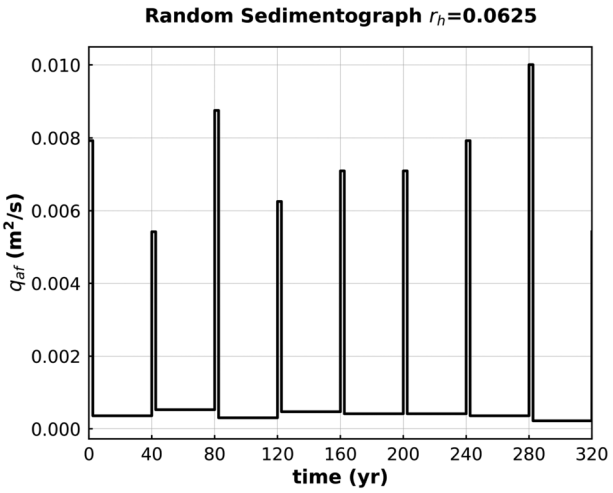


**Figure 4.** Randomized feed sedimentographs for $T$ = 40 years, over a period of 320 years. The vertical axis corresponds to the feed rate $q_{af}$ with $r_h$ = 0.0625 and $r_{qh}$ uniformly distributed in the range [6, 12].

A periodic sedimentograph provides a first look at the effect of varying sediment supply on alluvial/incisional morphodynamics. In nature, however, such delivery has a random element. Lague (2010) has emphasized the role of stochasticity of water discharge and sediment supply on incisional processes. Below we introduce stochasticity into sediment supply by letting $r_{qh}$ be a uniformly distributed random variable. More realistic probability distributions could easily be adopted, but uniformity is assumed for simplicity here. Illustrated in Figure 4 is such a series of sedimentographs for $T$ = 40 years, $r_h$ = 0.0625, and $r_{qh}$ randomly takes the values 6, 6.5, 7, 7.5,···, between 6 and 12.

## 3. Formulation of Morphodynamics

We treat incisional morphodynamics with the 1-D equation of bedrock volume conservation given below:

$$\frac{\partial \eta_b}{\partial t} = \upsilon - E, \tag{5}$$

where $\eta_b$ is bedrock elevation (averaged over local roughness variation as described below in Figure 5), $t$ is time, $\upsilon$ is rock uplift rate (assumed for simplicity to take a constant value here), and $E$ is the rate of incision into the bedrock. Here we assume that incision is caused by bedload clasts of specified size $D$ as they collide with the bedrock surface. It is further assumed that such collisions cause the removal of bedrock material but do not cause diminution of the bedload clasts.

We begin by reviewing the CSA (Zhang et al., 2015) closure for $E$ of Sklar and Dietrich (2004, 2006). In this innovative model, it is assumed that the transport of bedload at a rate that is below the capacity value (at which the bed would be fully alluviated) corresponds to zones of exposed bedrock. Let $q_a$ denotes the volume transport rate per unit width of alluvium (gravel moving as bedload herein), $q_{ac}$ denotes the capacity volume transport rate per unit width of gravel, $p$ denotes the areal fraction of bedrock surface that is covered by alluvium, and $\beta$ denotes a coefficient of bedrock wear with unit $L^{-1}$. The CSA relation for incision rate is

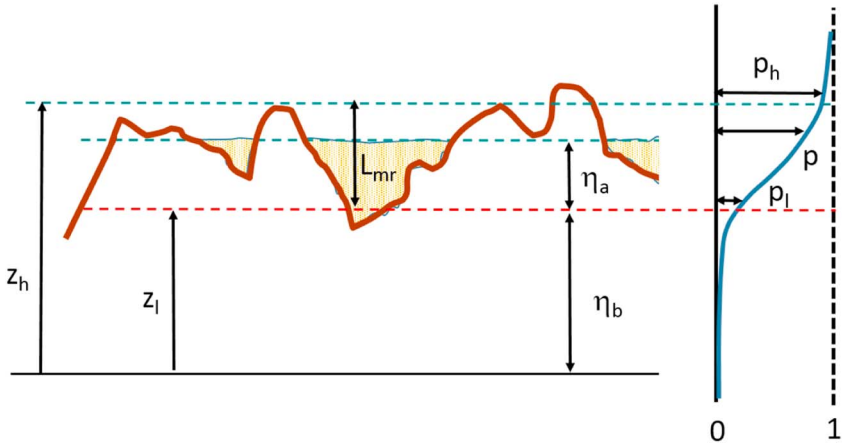


**Figure 5.** Definition diagram for macroroughness-based cover relation. A hypsometric curve of bedrock elevation is shown on the right. The parameter $p$ ($z$) corresponds to the fraction of the bedrock surface that is below elevation $z$. Note that the limit $p \to 1$ corresponds to an elevation $z$ that is far above the bedrock, and the limit $p \to 0$ corresponds to an elevation $z$ that is deep within the bedrock. Here $p_l$ denotes the areal fraction of a plane surface perpendicular to the page that is not in bedrock at elevation $z_l$ and $p_h$ denoting the areal fraction of a plane surface perpendicular to the page that is not in bedrock at elevation $z_h$. The macroroughness $L_{mr} = z_h - z_l$. The alluvial thickness $\eta_a$ is measured above elevation $z_l$, below which it is assumed that any alluvium is inaccessible to the flow. Bedrock thickness $\eta_b$ is measured from a datum to elevation $z_l$. The diagram illustrates alluvial fill to thickness $\eta_a$ and areal cover fraction $p$ associated with that thickness.

$$E = \beta q_{ac} p(1-p), \tag{6a}$$

where

$$p = \begin{cases} \dfrac{q_a}{q_{ac}}, & \dfrac{q_a}{q_{ac}} \le 1 \\ 1, & \dfrac{q_a}{q_{ac}} > 1 \end{cases}. \tag{6b}$$

The form of equation (6b) is supported by the experimental results of Chatanantavet and Parker (2008).

In Sklar and Dietrich (2004), the coefficient $\beta$ is a function of flow conditions. Zhang et al. (2015) have shown that for a wide range of conditions, however, $\beta$ can be approximated as constant (see Figures 9 and 10 therein). We adopt this approximation for simplicity.

The CSA formulation has been used to describe bedrock channel evolution by Sklar and Dietrich (2006) and Chatanantavet and Parker (2009). Equations (6a) and (6b), however, do not provide means for determining the transport rate $q_a$ at any point $x$ in the downstream direction. In consideration of this, we refer to the method as CSA-p, where $p$ denotes point formulation. Sklar and Dietrich (2006) and Chatanantavet and Parker (2009) introduce external relations to algebraically specify the downstream variation of $q_a$ in terms of sediment delivery from hillslopes in response to incision. Such a formulation, however, is not suited to handling the response of a reach to time-varying sediment input from, for example, hillslope failures driven by earthquakes or typhoons.

Zhang et al. (2015) overcame this problem by (a) reformulating the areal fraction cover so as to relate it to mean alluvial thickness $\eta_a$ over a rough bedrock surface with (characteristic) macroroughness $L_{\mathrm{mr}}$, as illustrated in Figure 5, and (b) adding an Exner equation of conservation of alluvium. Their relation for cover takes into account the statistics of local elevation variation of the bedrock surface itself. It takes the form

$$p = \begin{cases} p_l + (p_h - p_l)\dfrac{\eta_a}{L_{mr}} & 0 \le \dfrac{\eta_a}{L_{\mathrm{mr}}} \le \dfrac{1-p_l}{p_h - p_l} \\ 1 & \dfrac{\eta_a}{L_{\mathrm{mr}}} > \dfrac{1-p_l}{p_h - p_l} \end{cases}, \tag{7}$$

where $L_{\mathrm{mr}}$ is related to a measure of bedrock elevation spread (for example, standard deviation) on the hypsometric curve of bedrock elevation. The parameters $p_l$ and $p_h$ correspond to a characteristically low and a characteristically high probability on the hypsometric curve; here, as in Zhang et al. (2015), we use $p_l = 0.05$ and $p_h = 0.95$.

Zhang et al. (2015) derive the following equation for conservation of alluvium, which is also used here:

$$(1-\lambda) p \frac{\partial \eta_a}{\partial t} = -\frac{\partial}{\partial x}(q_{ac} p). \tag{8}$$

Here $\lambda$ denotes the porosity of the alluvium. They named their model the MRSAA model. In this model, bedrock morphodynamics are specifically linked to alluvial morphodynamics by means of the cover fraction $p$. This parameter must be known to implement equation (6a) for incision but is related to equation (8) governing alluvial morphodynamics via equation (7). Both the CSA and MRSAA models are intrinsically advective (through upstream-migrating knickpoint migration associated with incision) but only MRSAA is also intrinsically diffusive (through alluvial processes, as illustrated in detail in their paper). More elaboration on this point can be found in Zhang et al. (2015).

Zhang et al. (2015) illustrated four morphodynamic problems that can be captured with MRSAA but not with CSA-p: (a) stripping and emplacement of an alluvial layer over bedrock; (b) progression to a steady state at which incision and uplift balance after a bedrock reach is deeply flooded in alluvium; (c) 1-D morphodynamics of a horst graben, that is, a region of subsidence bounded upstream and downstream by regions of uplift; and (d) evolution of a bedrock river with an alluviated zone, and thus a migrating bedrock-alluvial transition, near a river mouth.

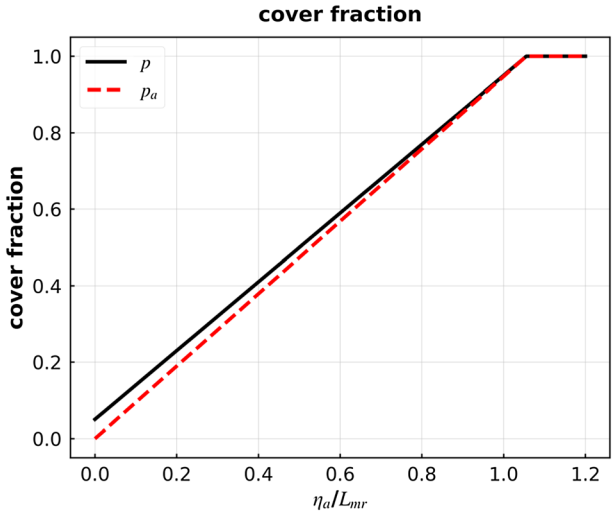


**Figure 6.** Plots of cover fraction $p$ and available cover fraction $p_a$ versus $\eta_a/L_{mr}$, computed from equations (7) to (9), respectively, using $p_l = 0.05$ and $p_h = 0.95$.

MRSAA is tailor made to study the effect of varying sediment supply (Zhang et al., 2013). The formulation contained there, however, contains several errors that have been corrected in Zhang et al. (2015). There is, however, one further small error in MRSAA that must be corrected before proceeding.

It is seen from equation (7) that $p$ equals a minimum nonzero value $p_l$ when the alluvial cover thickness $\eta_a = 0$. This condition was introduced to allow the formation of deep pockets of alluvium that are unavailable for mobilization into bedload transport. Such a formulation, however, allows for a small, unrealistic residual rate of incision even when the sediment transport rate drops to zero, that is, from equations (6a) and (7), $E = \beta q_{ac} p_l (1 - p_l)$. We correct this deficiency as follows:

$$p_a = \frac{p - p_l}{1 - p_l}, \tag{9}$$

where $p_a$ denotes the fraction of cover that is available for bedload transport. In Figure 6, we show plots of both $p$ and $p_a$ versus $\eta_a/L_{mr}$.

We accordingly modify equations (6a) and (8) to

$$E = \beta q_{ac} p_a (1 - p_a) \tag{10}$$

and

$$(1 - \lambda) p \frac{\partial \eta_a}{\partial t} = -\frac{\partial}{\partial x}(q_{ac} p_a). \tag{11}$$

We refer to the model defined by equations (7) and (9)–(11) as the corrected MRSAA model, that is, MRSAA-c.

## 4. Conditions for Calculations

### 4.1. Flow Hydraulics, Sediment Transport, and Flood Intermittency

We assume a channel with constant width $B$. In steep mountain streams, backwater effects are likely to be negligible (e.g., Parker, 2004). The normal (steady and uniform) flow assumption allows simplification. Let $Q$ denotes the water discharge during (morphodynamically active) flood flow occurring with intermittency $I$, $H$ denotes flood depth, $U$ denotes water velocity, $g$ denotes the acceleration of gravity, and $S_b$ denotes the streamwise bedrock surface slope, given as

$$S_b = -\frac{\partial \eta_b}{\partial x}. \tag{12}$$

Momentum and mass balance take the forms

$$\tau = \rho g H S_b, Q = UBH, \tag{13}$$

where $\tau$ is the boundary shear stress at flood flow and $\rho$ is the water density. The dimensionless Shields number $\tau^*$ and dimensionless Chezy resistance coefficient $Cz$ are defined as

$$\tau^* = \frac{\tau}{\rho R g D}, Cz = \frac{U}{\sqrt{\tau/\rho}}, \tag{14}$$

where $R$ denotes the submerged specific gravity of sediment (1.65 for quartz). As shown in Parker (2004) and Chatanantavet and Parker (2009), manipulating equations (12)–(14) yields the following relations for $H$ and $\tau^*$:

$$H = \left(\frac{Q^2}{Cz^2 gB^2 S_b}\right)^{1/3}, \quad \tau^* = \left(\frac{Q^2}{Cz^2 gB^2}\right)^{1/3} \frac{S_b{}^{2/3}}{RD}. \tag{15}$$

Capacity bedload transport is computed here using the modified form of Wong and Parker (2006a) of the relation of Meyer-Peter and Müller (1948). This relation is very similar to that of Fernandez Luque and van Beek (1976) used by Sklar and Dietrich (2006). It takes the form

$$q_{ac} = 4\sqrt{RgDD}\left(\tau^* - \tau_c^*\right)^{3/2}, \tag{16}$$

where $\tau_c^* = 0.0495$.

As noted above, we consider flood flow that prevails for time fraction $I$. With this in mind, we amend equations (10) and (11) to the respective forms

$$E = I\beta q_{ac} p_a (1 - p_a), \tag{17}$$

$$(1 - \lambda) p \frac{\partial \eta_a}{\partial t} = -I \frac{\partial}{\partial x}(q_{ac} p_a). \tag{18}$$

### 4.2. Boundary and Initial Conditions

As shown in Zhang et al. (2015), the formulation for bedrock morphodynamics, that is, equation (17), is first order in $x$, insofar as $q_{ac}$ depends on $S_b = -\partial \eta_b / \partial x$. It thus requires only one boundary condition. The example considered here is that of a downstream bedrock elevation, that is, base level is set to 0:

$$\eta_b|_{x=L} = 0. \tag{19}$$

The alluvial formulation of equation (18) is second order in $x$ via the term $\partial q_{ac}/\partial x \sim \partial S/\partial x \sim \partial^2 \eta / \partial x^2$, where $\eta = \eta_b + \eta_a$ = bed elevation, and thus requires two boundary conditions. The following boundary condition applies at upstream end of the reach, where $q_{af}(t)$ denotes a time-varying feed rate of alluvium

$$q_a|_{x=0} = q_{af}(t). \tag{20}$$

At the downstream end ($x = L$), a free boundary condition is applied for $\eta_a / L_{\mathrm{mr}} < 1$, and a fixed boundary condition is applied for $\eta_a / L_{\mathrm{mr}} \geq 1$:

$$(1 - \lambda) p \frac{\partial \eta_a}{\partial t} + I \frac{\partial (q_{ac} p_a)}{\partial x}\bigg|_{x=L} = 0 \quad \text{if} \quad \left[\frac{\eta_a}{L_{\mathrm{mr}}}\right]\bigg|_{x=L} < 1, \tag{21a}$$

$$\eta_a|_{x=L} = L_{\mathrm{mr}} \quad \text{if} \quad \left[\frac{\eta_a}{L_{\mathrm{mr}}}\right]\bigg|_{x=L} \geq 1. \tag{21b}$$

That is, equation (21a) specifies a free boundary in the case of partial alluvial cover, so allowing below-capacity sediment waves to exit the reach. Condition (21b), on the other hand, fixes the maximum downstream elevation at $\eta = \eta_a = L_{\mathrm{mr}}$.

The initial conditions used here are as follows:

$$\eta_b|_{t=0} = S_{bi}(L - x), \tag{22}$$

where $S_{\mathrm{bi}}$ denotes a constant initial bedrock slope, and

$$\eta_a|_{t=0} = \varphi_i L_{mr}, \tag{23}$$

so that the bed is covered with alluvium everywhere to a constant fraction $\varphi_i$ of the macroroughness height $L_{\mathrm{mr}}$.

**Table 2**
*Calculated Hydraulic and Sediment Transport Parameters at Bed Slope $S = S_b = 0.004$*

| Parameter | Definition | Value (s) |
|---|---|---|
| $H$ | Flood depth | 1.32 m |
| $Fr$ | Flood Froude number | 0.63 |
| $\tau^*$ | Flood Shields number | 0.16 m |
| $q_{ac}$ | Capacity bedload transport rate per unit width at flood flow | 0.0017 $m^2/s$ |

### 4.3. The Model Reach

The input parameters used in this paper are summarized in Table 1. In order to characterize a rapidly uplifting setting such as is found in Taiwan (e.g., Dadson et al., 2003), we set the rock uplift rate $\upsilon$ to a high value of 5 mm/year (MRSAA is applied to a wide range of input rates in Zhang et al., 2015). However, the bedrock underlying channel alluvium is exposed only intermittently in many mountain streams in Taiwan. For other parameters, then, we turn to a reach of the Shimanto River near Tokawa, Japan (Figure 2). The uplift rate is lower here, but localities where bedrock is extensively exposed are intermixed with localities with abundant alluvium. This allows estimation of both a characteristic alluvial substrate size and a bedrock macroroughness. Zhang et al. (2015) estimated the following input parameters, which are used for all of the numerical runs presented here: $Q = 300\ m^3/s$, $B = 100$ m, $D = 20$ mm, $Cz = 10$, $\lambda = 0.35$, $L_{mr} = 1$ m, and $I = 0.05$. These numbers are loosely based on the Shimanto River, Japan (Figure 2) as explained in Zhang et al. (2015). The abrasion coefficient $\beta$ is set to 0.05 $km^{-1}$, as justified in Zhang et al. (2015). We use an initial bedrock slope $S_{bi}$ of 0.004, again based loosely on the Shimanto River.

As shown in Table 2, the above numbers combined with equations (15) and (16) yield the values $H = 1.32$ m, Froude number $Fr = U/\sqrt{gH} = 0.63$, $\tau^* = 0.16$, and capacity bedload transport rate $q_{ac} = 0.00167\ m^2/s$. This capacity transport rate corresponds to $7.0 \times 10^5$ t/year.

In most of the runs presented below, we use a reach length $L$ of 20 km. Cases with $L = 60$ and 120 km are also considered. The parameter $\varphi_i$ specifying the initial alluvial cover is set to 0.5 for most runs.

## 5. Results of Calculations

In this section we perform numerical calculations in which equations (17) and (18) are solved, subject to the initial and boundary conditions above, until a steady state balance between uplift and incision is achieved. We use as a reference mean sediment rate $q_{af,m} = 0.000834\ m^2/s$, that is, half the capacity value corresponding to the initial bedrock slope. Using the parameters of Table 1, this feed rate is found to correspond to $3.5 \times 10^5$ t/year (= 0.000834 $m^2/s \times 100$ m $\times$ 2.65 $t/m^3 \times$ (365.25 $\times$ 24 $\times$ 60 $\times$ 60) s/year $\times$ 0.05 [intermittency]). More specifically, we consider sedimentographs for which the high feed rate is $r_{qh} \times q_{af,m}$ and the low feed rate is $r_{ql} \times q_{af,m}$, such that the average over the sedimentograph is $q_{af,m}$, in accordance with equations (3) and (4).

### 5.1. Constant Sediment Feed Rate

The appropriate place to start is a constant feed rate, that is, $r_{qh} = 1$. Figure 7a shows the time evolution of the bedrock elevation profile of a reach with a length of 20 km to steady state, which is achieved by $t = 1{,}000$ years. Results are shown for both CSA-p (no alluvial advection/diffusion, solid lines) and MRSAA-c (includes alluvial advection/diffusion, dashed lines). In the case of CSA-p, steady state is achieved by the purely advective process of upstream knickpoint migration. In Figure 7a, the difference between CSA-p and MRSAA-c is nearly indistinguishable. It can be seen in the expanded view in Figure 7b, however, that MRSAA renders the knickpoint as a short knickzone. This reflects the role of alluvial diffusion, in addition to bedrock advection in MRSAA-c.

In Figures 8a and 8b, we show the time evolution of the cover fractions $p$ and $p_a$ to steady state. In the case of CSA-p, shown in Figure 8a, we see an upstream-migrating front of cover fraction $p$, with the value jumping from the initial value of 0.5 to the steady state value of 0.924 necessary to allow incision to balance uplift. The small jumps are artifacts that are characteristic of a model with advection but no diffusion. In the case of MRSAA-c, shown in Figure 8b, the front is more diffuse, but the steady state value of $p_a$ is also 0.924.

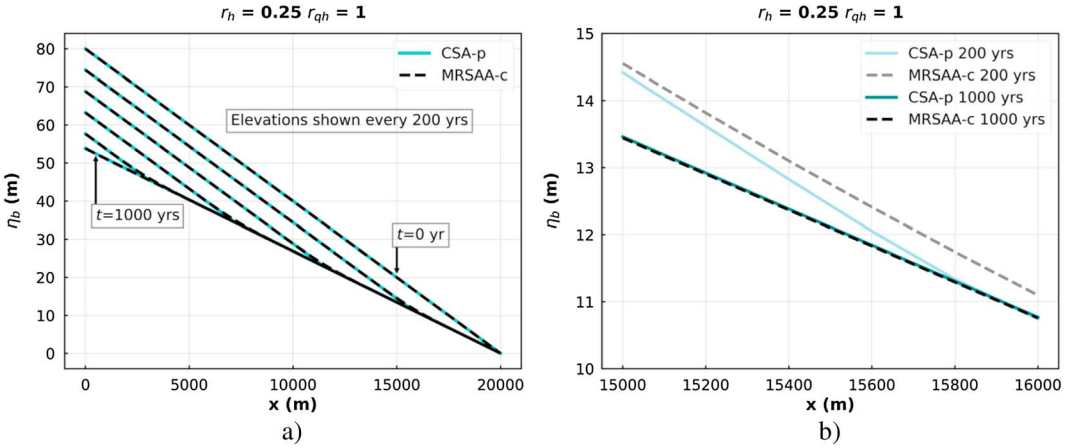


**Figure 7.** Evolution of bedrock elevation to a steady state balance between incision and uplift for reach length $L$ = 20 km and a constant feed rate $q_{af,m}$ = 0.000834 m$^2$/s (3.5 × 10$^5$ t/year), that is, $r_{qh}$ = 1. (a) Results for CSA-p (no alluvial advection/diffusion, solid lines) and MRSAA-c (with alluvial advection/diffusion, dashed lines). (b) Zoom into Figure 7a for $x$ between 15,000 and 16,000 m and $\eta_b$ between 10 and 15 m. In CSA-p, the steady state is realized by means of an upstream-migrating knickpoint. In MRSAA-c, diffusive effects associated with alluvial morphodynamics result in a knickzone rather than a knickpoint, which can be seen in the expanded view of Figure 7b. Otherwise, the results are very similar, both reaching a steady state bedrock slope $S_{bs}$ that is spatially constant and equal to 0.0027. CSA-p = Capacity Saltation Abrasion, where $p$ denotes point formulation; MRSAA-c = corrected Macroroughness Saltation-Abrasion-Alluviation model.

### 5.2. Repeated Sedimentograph With $T$ = 40 Years, $T_h$ = 10 Years, and $r_{qh}$ = 3

We now consider a repeated sedimentograph with a duration $T$ = 40 years, duration of high feed $T_h$ = 10 years ($r_h$ = 0.25), duration of low feed $T_l$ = 30 years, and the ratio of high feed rate to mean feed rate $r_{qh}$ = 3, such that according to equations (3) and (4) the high feed rate $q_{af,h}$ = 0.002502 m$^2$/s (1.0 × 10$^6$ t/year) and the low feed rate $q_{af,l}$ = 0.000278 m$^2$/s (1.2 × 10$^5$ t/year). Again, the reach length is $L$ = 20 km. In this case, the results for CSA-p (no alluvial advection/diffusion) and MRSAA-c (with alluvial advection/diffusion) show a remarkable difference, as illustrated in the plots of bedrock elevation $\eta_b$ given in Figure 9a (CSA-p) and Figure 9b (MRSAA-c). The respective reach-averaged steady state bedrock slopes $S_{bm}$ are 0.0017 and 0.0027.

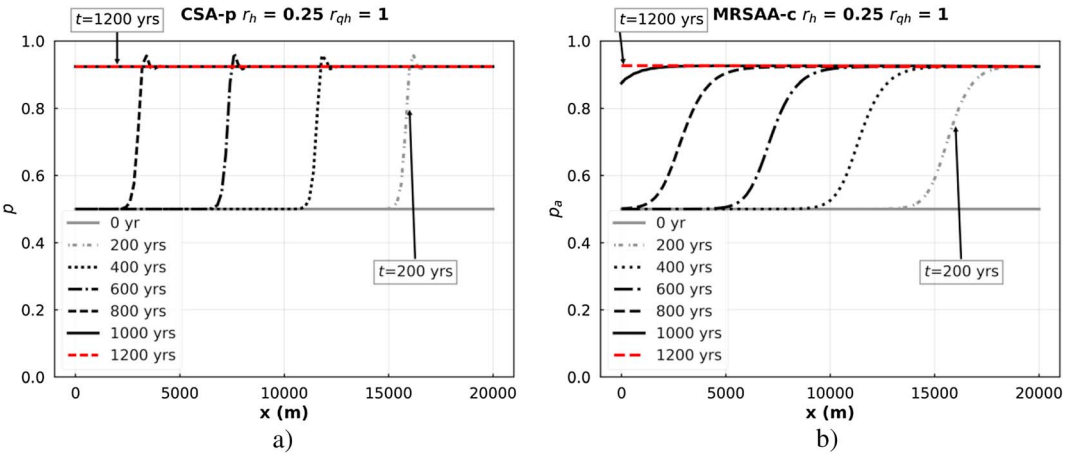


**Figure 8.** Evolution of cover fraction to a steady state balance between incision and uplift for $L$ = 20 km and a constant feed rate $q_{af}$ = 0.000834 m$^2$/s (3.5 × 10$^5$ t/year), corresponding to $r_{qh}$ = 1. (a) Results for cover fraction $p$ for CSA-p (no alluvial advection/diffusion); (b) results for available cover fraction $p_a$ for MRSAA-c (with alluvial advection/diffusion). Figure 8a documents an increase of cover fraction $p$ from 0.5 to 0.924 by the upstream-migrating knickpoint. Figure 8b documents an increase of available cover fraction $p_a$ from 0.47 to 0.924 by the more diffuse upstream-migrating knickzone. CSA-p = Capacity Saltation Abrasion, where $p$ denotes point formulation; MRSAA-c = corrected Macroroughness Saltation-Abrasion-Alluviation model.

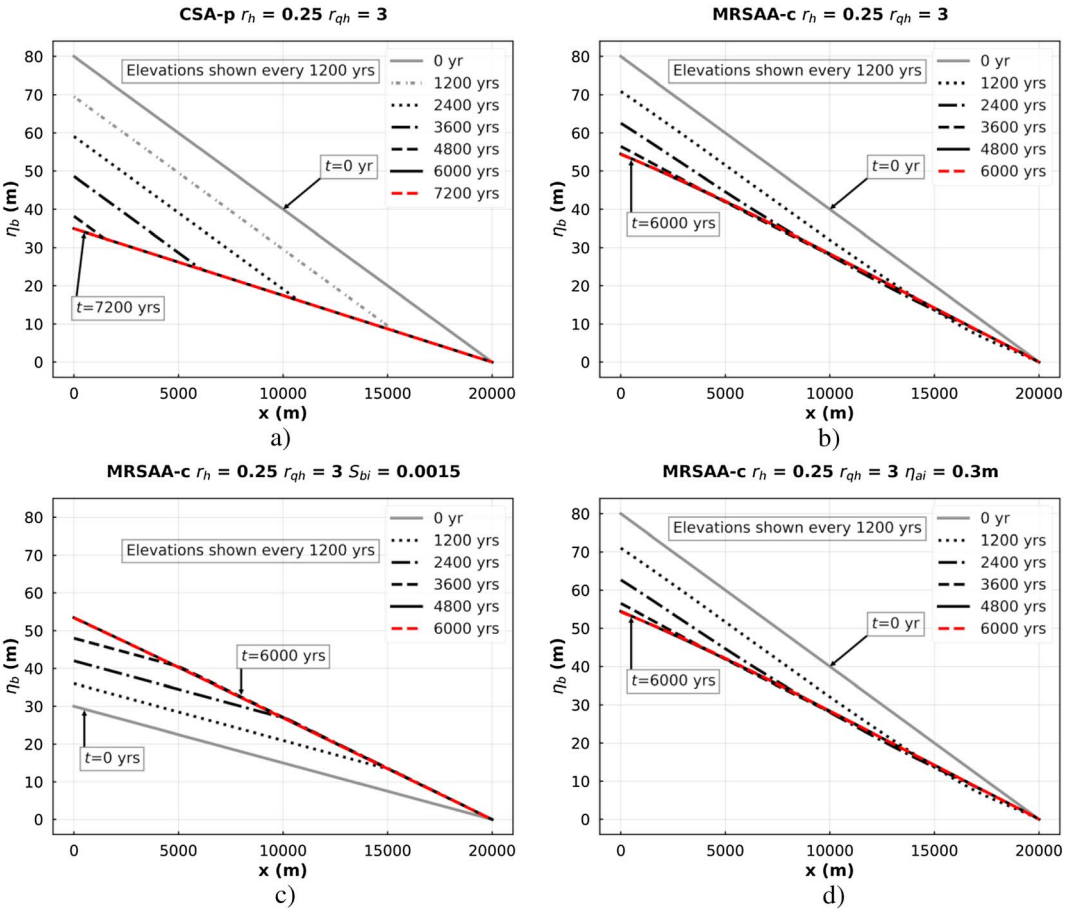


**Figure 9.** Evolution to a steady state balance between incision and uplift for a repeated sedimentograph of duration $T$ = 40 years, with $L$ = 20 km and $r_h$ = 0.25 (that is, 10 years of high feed). The mean feed rate $q_{af,m}$ = 0.000834 $m^2/s$ ($3.5 \times 10^5$ t/year) and $r_{qh}$ = 3. (a) Results for bedrock elevation $\eta_b$ using CSA-p (no alluvial advection/diffusion), initial bedrock slope $S_{bi}$ = 0.004, and initial alluvium depth $\eta_{ai}$ = 0.5 m, that is, ($S_{bi}$, $\eta_{ai}$) = (0.004, 0.5 m); (b) results for bedrock elevation $\eta_b$ using MRSAA-c (with alluvial advection/diffusion) and the initial values ($S_{bi}$, $\eta_{ai}$) = (0.004, 0.5 m); (c) results for bedrock elevation $\eta_b$ using MRSAA-c and the initial values ($S_{bi}$, $\eta_{ai}$) = (0.0015, 0.5 m); (d) results for bedrock elevation $\eta_b$ using MRSAA-c and the initial values ($S_{bi}$, $\eta_{ai}$) = (0.004, 0.3 m). Here Figures 9a and 9b correspond to the results of different models (CSA-p and MRSAA-c, respectively) under the same initial conditions. Figures 9c and 9d show results from the MRSAA-c model, but starting from initial parameters $S_{bi}$ and $\eta_{ai}$ that differ from those used in Figure 9b. However, all three cases modeled with MRSAA-c, that is, Figures 9b–9d converge to the same steady state bedrock slope of 0.0027. The upstream steady state elevation for MRSAA-c is 54.9 m in Figures 9b–9d, that is, very close to the value of 53.8 m for constant feed rate (Figure 7b). The corresponding upstream elevation for CSA-p is substantially lower at 34.9 m in Figure 9a. CSA-p = Capacity Saltation Abrasion, where *p* denotes point formulation; MRSAA-c = corrected Macroroughness Saltation-Abrasion-Alluviation model.

In the case of MRSAA-c, shown in Figure 9b, the steady state bedrock elevation profile for $r_{qh}$ = 3 is quite similar (but not identical, as we show below) to that for a constant feed rate ($r_{qh}$ = 1: Figures 7a and 7b), although significantly more time is required to achieve it. In the case of CSA-p, however, the steady state elevation profile has the substantially lower slope shown in Figure 9a. We explain this difference below; suffice it to note here that the alluvial diffusion in MRSAA-c acts to spread out the supplied sediment downstream.

Figure 9c shows a case using MRSAA-c that is the same as the case of Figure 9b except that $S_{bi}$ = 0.0015 rather than 0.004. This is done to study the effect of initial slope on the morphodynamics and final steady state. It can be seen from Figures 9b and 9c that the final steady state, for which $S_{bm}$ = 0.0027, is independent of the initial slope. Figure 9d shows a case using MRSAA-c that is the same as Figure 9b except that the initial depth of alluvium $\eta_{ai}$ = 0.3 m rather than 0.5 m. Again, the same steady state profile is obtained regardless of the initial alluvium depth.

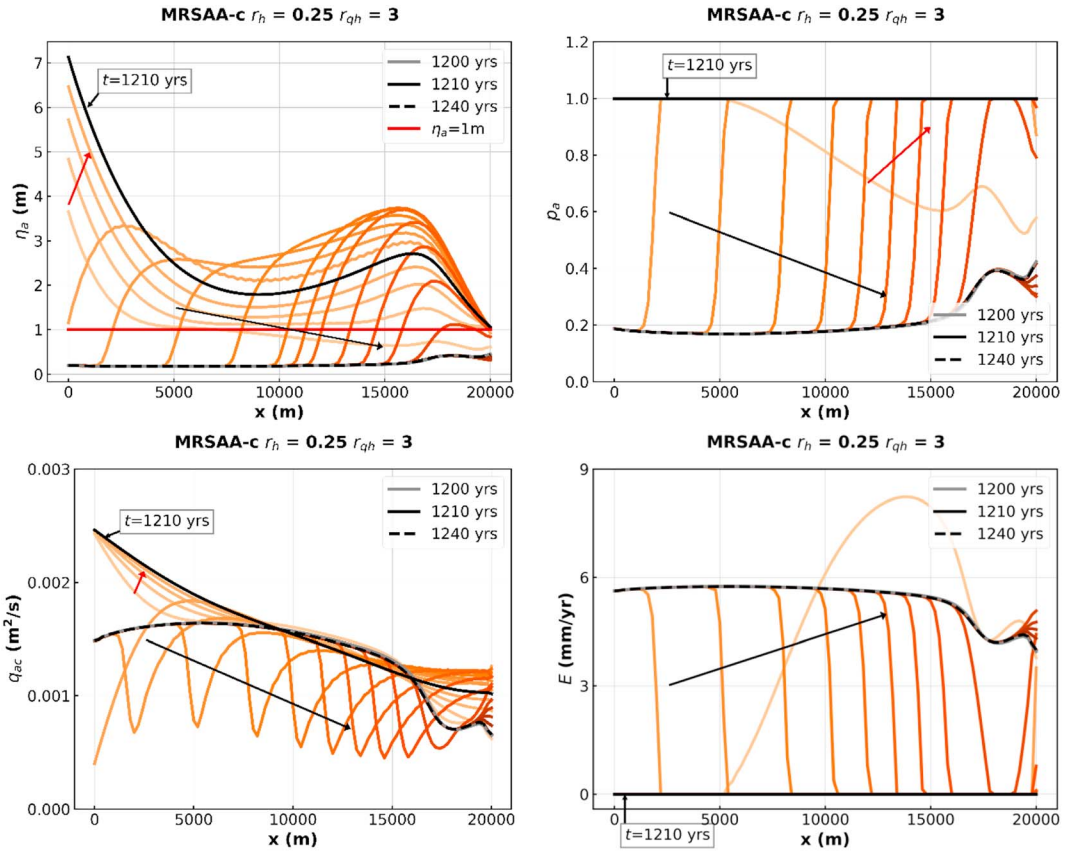


**Figure 10.** (a–d) Results corresponding to Figure 9b for $\eta_a$, $p_a$, $q_{ac}$, and $E$, respectively, for a sedimentograph cycle 1,200–1,240 years (before macroscopic steady state is reached). Each line in Figures 10a–10d shows every 2 years of sedimentograph. The red arrows in Figures 10a–10c denote the direction of change from 1,200 to 1,210 years (high feed rate), and the black arrows denote the direction of change from 1,210 to 1,240 years (low feed rate). The red horizontal line in Figure 10a denotes the macroroughness height $L_{mr}$, which is just covered when $\eta_a$ = 1 m. CSA-p = Capacity Saltation Abrasion, where *p* denotes point formulation; MRSAA-c = corrected Macroroughness Saltation-Abrasion-Alluviation model.

Figures 10a and 10d illustrate the time evolution to macroscopic steady state. All calculations are based on the parameters used for Figure 9b. Figures 10a–10d show the morphodynamic response over one complete sedimentograph cycle, before macroscopic steady state is reached. Specifically, the figures show how alluvial thickness $\eta_a$ (Figure 10a), available cover fraction $p_a$ (Figure 10b), capacity sediment transport rate $q_{ac}$ (Figure 10c), and incision rate $E$ (Figure 10d) vary over the sedimentograph cycle corresponding to 1,200–1,240 years. In Figure 10a, it can be seen that alluvial thickness $\eta_a$ fluctuates between 0.18 and nearly 7.13 m. Figure 10b similarly documents the fluctuation of cover fraction $p_a$ between about 0.2 and 1 (complete alluviation). Figure 10c documents how the fluctuations of the capacity sediment transport rate $q_{ac}$ persist throughout most of the reach. Note in Figure 10d that in the period 1,200–1,240 years (before macroscopic steady state is reached), the incision rate $E$ spends a significant time at the value 0 (complete alluviation) but varies as high as nearly 9 mm/year, a value that exceeds the uplift rate of 5 mm/year.

Figures 11a–11d show the corresponding plots for $\eta_a$, $p_a$, $q_{ac}$, and $E$ as they vary over a complete cycle (6,000–6,040 years) after macroscopic equilibrium has been reached. Figure 11a shows that alluvial thickness $\eta_a$ varies between 0.3 and 12.9 m upstream, and that this variation is strongly damped downstream. Figure 11b shows the pattern of cyclic variation in cover fraction $p_a$. Figure 11c shows that the capacity sediment transport rate $q_{ac}$ is strongly damped downstream at macroscopic equilibrium. Figure 11d similarly documents how the incision rate $E$ varies over one cycle, just such that the mean rate (5 mm/year) equals the uplift rate of 5 mm/year. In totality Figures 10 and 11 allow visualization of the evolution and establishment of macroscopic equilibrium.

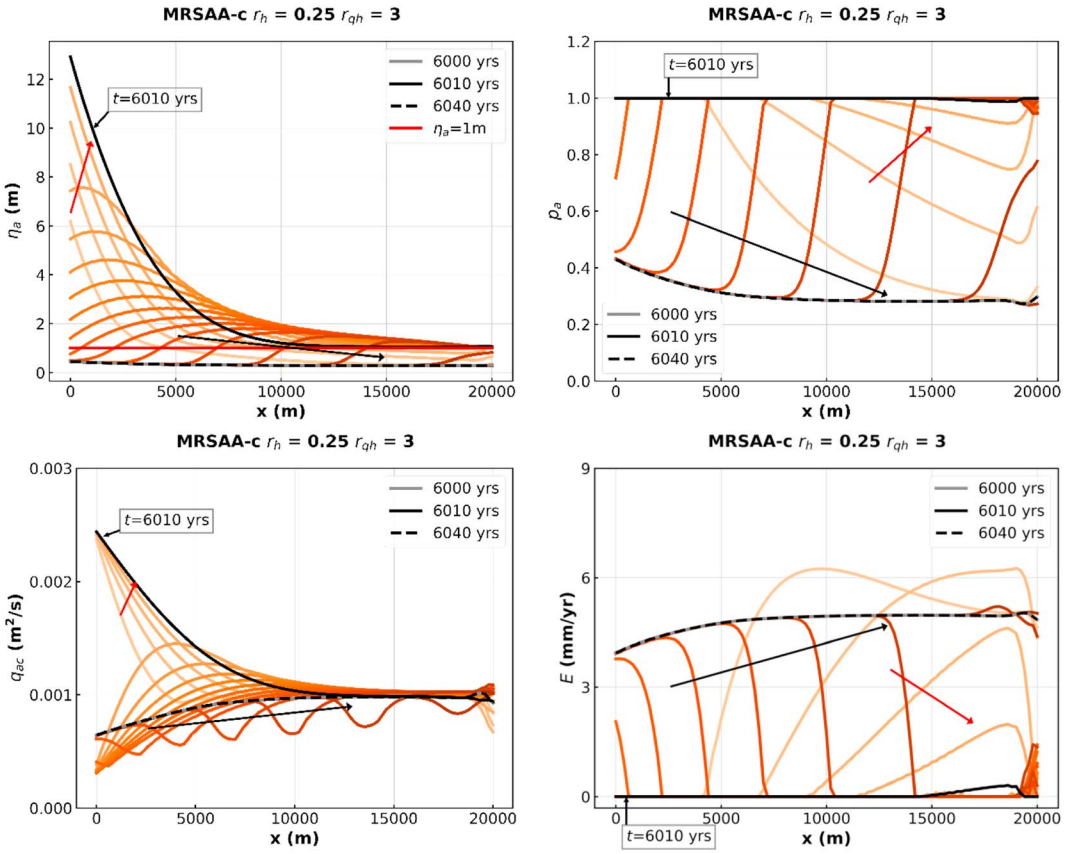


**Figure 11.** (a–d) Results corresponding to the conditions of Figure 9b, for $\eta_a$, $p_a$, $q_{ac}$, and $E$, over the sedimentograph cycle 6,000–6,040 years (after macroscopic steady state is reached). Each line in Figures 11a–11d shows every 2 years of sedimentograph. The red horizontal line in Figure 11a denotes the macroroughness height $L_{mr}$ = 1 m. The red arrows in Figures 11a–11d denote the direction of change over the first 10 years (that is, 6,000–6,010 years with high feed rate). The black arrows denote the corresponding direction of changes over the last 30 years of the sedimentograph (that is, 6010–6040 years with low feed rate). CSA-p = Capacity Saltation Abrasion, where *p* denotes point formulation; MRSAA-c = corrected Macroroughness Saltation-Abrasion-Alluviation model.

We compare the steady state bedrock slope profiles corresponding to CSA-p with $r_{qh}$ = 1, CSA-p with $r_{qh}$ = 3, and MRSAA-c with $r_{qh}$ = 3 in Figure 12. In the case of CSA-p, the steady state slope is spatially constant, regardless of whether $r_{qh}$ = 1 (constant feed rate) or 3 (high feed rate that is 3 times the mean feed rate). The slight fluctuations often seen at the downstream end of the reach are numerical artifacts. The steady state slopes $S_{bs}$ for CSA-p are, however, dramatically different; that is, $S_{bs,m}$ = 0.0027 for $r_{qh}$ = 1 but 0.0017 for $r_{qh}$ = 3. In the case of MRSAA-c, the reach-averaged steady state slope $S_{bs,m}$ is close to the value 0.0027 for constant feed rate, but $S_{bs}$ varies systematically with streamwise distance $x$. Specifically, bedrock slope is notably depressed below the constant feed case over the first 5,000 m of the reach but is somewhat elevated farther downstream.

We have illustrated in the preceding text two features of interest. First, for a sedimentograph with $r_h$ = 0.25 and $r_{qh}$ = 3, CSA-p (no alluvial advection/diffusion) predicts a steady state bedrock slope that is well below the value for constant feed rate, whereas MRSAA-c (with alluvial advection/diffusion) predicts a reach-averaged bedrock slope that is about the same. Second, in the case of MRSAA-c, steady state bedrock slope varies systematically in the downstream direction. The reason for this difference can be found in the spatiotemporal variation of the sediment transport rate $q_a$. Figure 13 shows the temporal variation of $q_a$ over one cycle at the upstream and downstream ends of the reach, for MRSAA-c applied to the case described above ($r_h$ = 0.25, $r_{qh}$ = 3). It can be seen that a spiky sedimentograph at the upstream end has been diffused away to a sediment transport rate $q_a$ that is roughly constant at the downstream end. The zone of low bedrock slope in

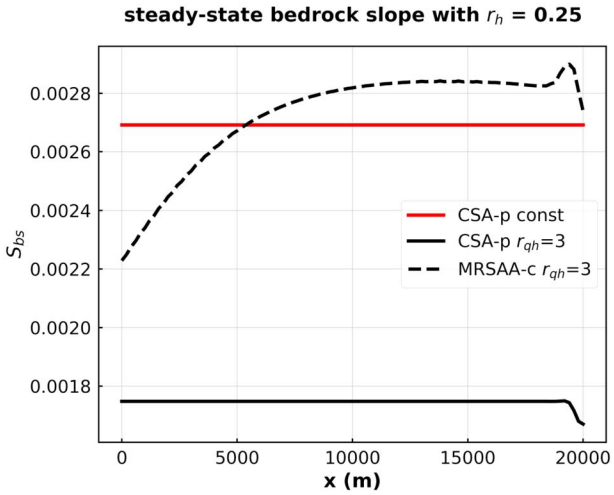


**Figure 12.** Steady state bedrock slope ($S_{bs}$) profiles for three cases for which $T$ = 40 years and $q_{af,m}$ = 0.00083 m$^2$/s: CSA-p (no alluvial advection/diffusion) with constant feed (denoted as CSA-p const); CSA-p (no alluvial advection/diffusion) with $r_h$ = 0.25 and $r_{qh}$ = 3 (denoted as CSA-p $r_{qh}$ = 3); and MRSAA-c (with alluvial advection/diffusion) with $r_h$ = 0.25 and $r_{qh}$ = 3 (denoted as MRSAA-c $r_{qh}$ = 3). The spatially averaged bedrock slope $S_{bs,m}$ for MRSAA-c is nearly the same as that for CSA-p with constant feed, that is, 0.0027. The bedrock slope $S_{bs}$ for CSA-p with $r_{qh}$ = 3 is much lower, taking the constant value 0.0017. Here $L$ = 20 km. CSA-p = Capacity Saltation Abrasion, where $p$ denotes point formulation; MRSAA-c = corrected Macroroughness Saltation-Abrasion-Alluviation model.

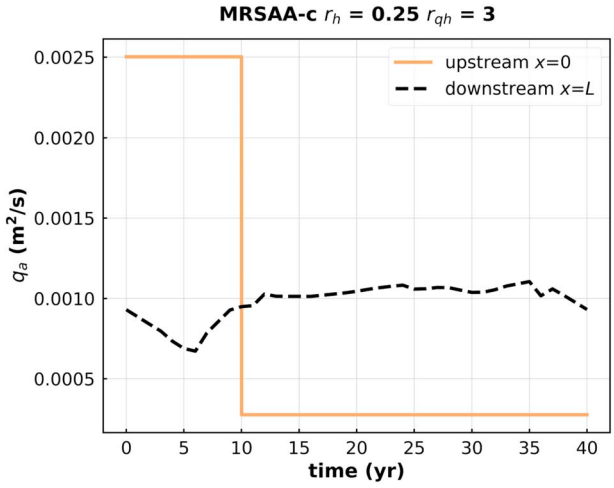


**Figure 13.** Upstream (feed) sedimentograph and downstream ($L$ = 20 km) sedimentograph at steady state for MRSAA-c (with alluvial advection/diffusion) with $q_{af,m}$ = 0.000834 m$^2$/s (3.5 × 10$^5$ t/year), $T$ = 40 years, $r_h$ = 0.25, and $r_{qh}$ = 3. In the corresponding case for CSA-p (no alluvial advection/diffusion), the feed sedimentograph is the same, and the downstream sedimentograph is the same as that for the feed. In the case of MRSAA-c, the peaky sedimentograph has been diffused into near uniformity, explaining why the mean steady state slope is nearly the same as for the case of constant feed (see Figure 16 below). CSA-p = Capacity Saltation Abrasion, where $p$ denotes point formulation; MRSAA-c = corrected Macroroughness Saltation-Abrasion-Alluviation model.

the upstream 5 km of Figure 12 is responding to a transport rate $q_a$ that varies strongly in time, whereas the zone in the last 10 km is responding to a transport rate that varies little in time. In the case of CSA-p, however, the same peaky sedimentograph propagates all the way downstream.

To find out the reason for this difference, we consider the steady state form of equation (5) using CSA-p, that is, equation (6), and MRSAA-c, that is, equation (10). The respective forms with flood intermittency $I$ are

$$v = I\beta q_{ac}\overline{p(1-p)} \tag{24}$$

and

$$v = I\beta q_{ac}\overline{p_a(1-p_a)}, \tag{25}$$

where the overbar denotes averaging over the reach and a single cycle. In the case of MRSAA-c, this average is computed as follows, where $A$ is an arbitrary parameter:

$$\overline{A} = \frac{1}{T}\frac{1}{L}\int_0^T\int_0^L A dt dx. \tag{26}$$

In the case of CSA-p, however, the sedimentograph for any value of $x$ is the same as at the feed point, so that equation (26) simplifies to

$$\overline{A} = \frac{1}{T}\int_0^T A dt. \tag{27}$$

In equation (25) for CSA-p, the capacity transport rate $q_{ac}$ has been extracted from the average, since it is constant in space and time at steady state.

Table 3 summarizes calculated steady state values of $\overline{p}$, $\overline{p(1-p)}$, $\overline{q_{ac}}$, $\overline{q_{ac}p(1-p)}$, $\overline{q_{ac}}\times\overline{p(1-p)}$, and mean steady state bedrock slope $S_{bs,m}$ using CSA-p with $r_h$ = 0.25 and $r_{qh}$ varying from 1 to 4, and $\overline{p_a}$, $\overline{p_a(1-p_a)}$, $\overline{q_{ac}}$, $\overline{q_{ac}p_a(1-p_a)}$, $\overline{q_{ac}}\times\overline{p_a(1-p_a)}$, and $S_{bs,m}$ using MRSAA-c, again with $r_h$ = 0.25 and $r_{qh}$ = 4. Also shown are the values for the corresponding cases for which the sediment feed rate is held constant at 4 times the mean value of the other cases, that is, 4 × $q_{af,m}$. It should be noted that in CSA-p, both $q_{ac}$ and $S_{bs}$ are in fact constant in space at steady state. Here we focus on the values for $r_{qh}$ = 1 and 3 in Table 3; other values are considered below.

Both MRSAA-c (with advection-diffusion) and CSA-p (no advection/diffusion) for the ratio of high feed rate to mean feed rate $r_{qh}$ = 3 give the same values for $\overline{q_{ac}}\times\overline{p(1-p)}\cong\overline{q_{ac}p_a(1-p_a)}$ = 6.34 × 10$^{-5}$ m$^2$/s necessary to equal the uplift rate $\upsilon$ of 5 mm/year when multiplied by $I\beta$. The value for $q_{ac}$ for CSA-p is 0.000399 m$^2$/s (1.7 × 10$^5$ t/year). In MRSAA-c, $q_{ac}$ varies only mildly at steady state; its average value $\overline{q_{ac}}$ is 0.00101 m$^2$/s (4.2 × 105 t/year). There is also a difference between $\overline{p(1-p)}$ for CSA-p and $\overline{p_a(1-p_a)}$ for MRSAA-c; the corresponding values are 0.159 in the former case and 0.071 in the latter case.

**Table 3**
*Values of Parameters Related to Incision Computed From CSA-p and MRSAA-c*

| | $r_{qh}$ | $\overline{p}$ | $\overline{p(1-p)}$ | $\overline{q_{ac}}$ | $\overline{q_{ac}p(1-p)}$ | $\overline{q_{ac}}\times\overline{p(1-p)}$ | $S_{bs,m}$ |
|---|---|---|---|---|---|---|---|
| CSA-p | 1 | 0.924 | 0.070 | 0.000903 | $6.34\times10^{-5}$ | $6.34\times10^{-5}$ | 0.0027 |
| | 3 | 0.772 | 0.159 | 0.000399 | $6.34\times10^{-5}$ | $6.33\times10^{-5}$ | 0.0017 |
| | 4 | 0.231 | 0.018 | 0.003611 | $6.34\times10^{-5}$ | $6.34\times10^{-5}$ | 0.0071 |
| | $4\times q_{af,m}$ | 0.981 | 0.019 | 0.003401 | $6.34\times10^{-5}$ | $6.34\times10^{-5}$ | 0.0068 |
| | $r_{qh}$ | $\overline{p_a}$ | $\overline{p_a(1-p_a)}$ | $\overline{q_{ac}}$ | $\overline{q_{ac}p_a(1-p_a)}$ | $\overline{q_{ac}}\times\overline{p_a(1-p_a)}$ | $S_{bs,m}$ |
| MRSAA-c | 1 | 0.924 | 0.070 | 0.000902 | $6.32\times10^{-5}$ | $6.32\times10^{-5}$ | 0.0027 |
| | 3 | 0.807 | 0.071 | 0.001009 | $6.34\times10^{-5}$ | $7.11\times10^{-5}$ | 0.0027 |
| | 4 | 0.245 | 0.017 | 0.003737 | $6.34\times10^{-5}$ | $6.36\times10^{-5}$ | 0.0073 |
| | $4\times q_{af,m}$ | 0.981 | 0.019 | 0.003401 | $6.34\times10^{-5}$ | $6.34\times10^{-5}$ | 0.0068 |

*Note.* The notation $4\times q_{af,m}$ is short hand for a constant feed rate at 4 times the mean value for the corresponding sedimentograph, that is, with $r_h = 0.25$. The overbar denotes spatiotemporal averaging over one cycle at steady state. The units of $q_{ac}$ are square meter per second.

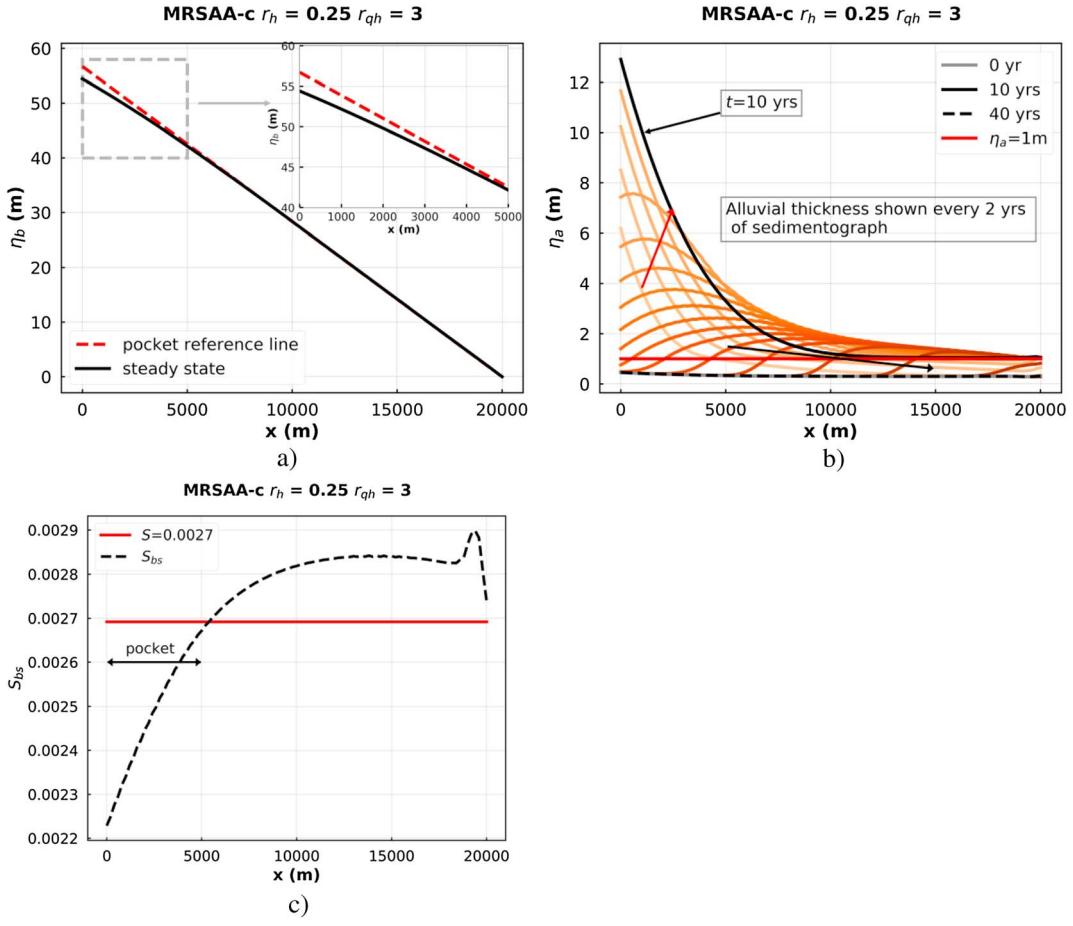


**Figure 14.** The steady state for MRSAA-c with $L = 20$ km, $q_{af,m} = 0.000834$ m$^2$/s ($3.5\times10^5$ t/year), $T = 40$ years, $r_h = 0.25$, and $r_{qh} = 3$ is characterized by a *pocket* of low elevation toward the upstream, corresponding to low bedrock slope $S_{bs}$ in Figure 14c. (a) Steady state profile of bedrock elevation, along with the bedrock elevation profile extrapolated from the nearly constant bedrock slope for the downstream half of the domain. This latter profile is denoted as the pocket reference line. The first 5,000 m of Figure 14a is expanded in the upper right of the panel to better show the pocket; (b) cyclic variation of profiles of alluvial thickness over one sedimentograph ($T = 40$ years) after steady state for this case. Thickness varies by as much as 12.9 m in the pocket but shows much less variation beyond $x = 10$ km; (c) bedrock slope $S_{bs}$ versus distance $x$. Profiles are shown for $r_h = 0.25$ and $r_{qh} = 3$, along with the corresponding line for a constant feed rate ($S = 0.0027$). The red line, red arrow, and black arrow in Figure 14b have the same meaning as in Figures 10 and 11. MRSAA-c = corrected Macroroughness Saltation-Abrasion-Alluviation model.

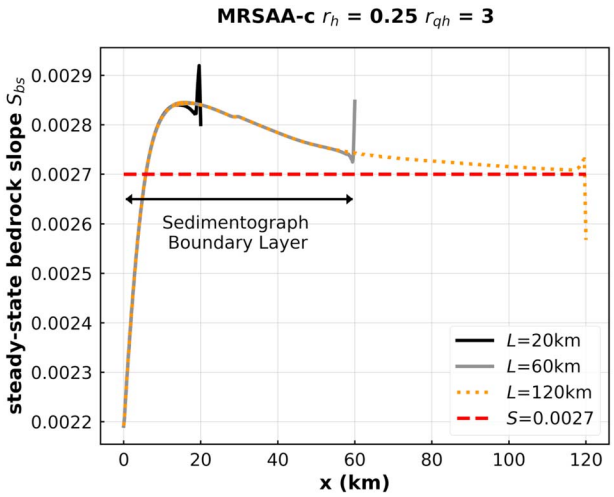


**Figure 15.** Steady state profiles of bed slope $S_{bs}$ for MRSAA-c with $q_{af,m}$ = 0.000834 $m^2$/s (3.5 × $10^5$ t/year), $T$ = 40 years, $r_h$ = 0.25, and $r_{qh}$ = 3. Three reach lengths are included, that is, $L$ = 20, 60, and 120 km. It can be seen that the profile is universal in form and thus is invariant to reach length; the profile for a shorter reach plots on top of that for a longer reach. The diagram allows identification of an upstream sedimentograph *boundary layer* within which most of the effects of the sedimentograph are confined. This boundary is associated with the action of diffusive alluvial morphodynamics to damp the sedimentograph and thus does not arise in CSA-p. CSA-p = Capacity Saltation Abrasion, where *p* denotes point formulation; MRSAA-c = corrected Macroroughness Saltation-Abrasion-Alluviation model.

Now we return to the reference case of a constant feed rate, that is, $r_{qh}$ = 1 (Figures 7 and 8). For this case, CSA-p and MRSAA-c give very nearly the same answer. More specifically, for CSA-p, the steady state values of $q_{ac}$ and $\overline{p(1-p)}$ are 0.000903 $m^2$/s (3.8 × $10^5$ t/year) and 0.070, respectively. These values are close to the values of $\overline{q_{ac}}$ and $\overline{p_a(1-p_a)}$ from MRSAA-c for $r_{qh}$ = 3 but different from the corresponding values from CSA-p for $r_{qh}$ = 3. Evidently the effect of diffusion in MRSAA-c smears out the sedimentograph over a sufficiently large part of the domain so that the morphodynamics becomes similar to the case of constant feed.

This smearing of the sedimentograph in MRSAA-c, however, occurs only after some distance downstream of the feed point. Two points are of interest in this regard. In Figures 14a, we show two lines of elevation. One, labeled *steady state*, is the steady state solution for bedrock elevation $\eta_b$ for MRSAA with $r_{qh}$ = 3. The other, labeled *pocket reference line*, is a straight line corresponding to an upstream extrapolation of the reach of near-constant bedrock slope in the downstream part of the domain. This terminology is chosen because the two lines in Figure 14a highlight the existence of a *pocket* or zone of locally depressed bedrock slope and elevation near the upstream end. This pocket can also be seen in terms of reduced bedrock slope toward the upstream end in Figure 12. The pocket corresponds to about 4.2% of the total drop in the elevation over the 20-km longitudinal profile.

This pocket is associated with a thickness of alluvial cover $\eta_a$ that cyclically varies from 0.3 to 12.9 m at the upstream end at steady state (Figure 14b). That is, a thick layer of alluvium is cyclically emplaced and evacuated, in a way reminiscent of the landslides in Figures 1a–1c. The pocket represents the morphodynamic adjustment of the bedrock to this *pumping* of alluvium induced by the sedimentograph. The minimum value of cover fraction *p* over the sedimentograph is 0.3.

### 5.3. Effect of Increasing Reach Length

Here we use the same case as in the previous section, that is, $T$ = 40, $T_h$ = 10 years ($r_h$ = 0.25), $T_l$ = 30 years, and $r_{qh}$ = 3, but now we vary the reach length. Figure 15 shows profiles for steady state bedrock slope $S_{bs}$ for $L$ = 20, 60, and 120 km. Also included for reference is the constant slope for the case $r_{qh}$ = 1 (constant feed). It is seen that the profiles for $L$ = 20 and 60 km are simply truncated versions of the profile for $L$ = 120 km. Sufficiently far downstream, the bedrock slope approaches the value corresponding to constant feed rate, again underlining the importance of diffusion. Upstream, a distinct *sedimentograph boundary layer*, within which the effects of feed variation are confined, can be identified. We use this terminology in analogy to the *hydrograph boundary layer* identified in Wong and Parker (2006b), Parker et al. (2007), An, Cui, et al. (2017), and An, Fu, et al. (2017), according to which the effects of temporally fluctuating discharge (and by extension sediment feed) can be restricted to a short upstream fraction of total reach length. Wong and Parker (2006b) outline the mathematics of the hydrograph boundary layer in some detail. The length of this boundary layer depends on how it is defined (that is, the distance at which the relative difference between the bedrock slope and its value for constant feed drops to a prescribed value), but Figure 15 suggests a value of about 60 km. The key point here is that the effect of the sedimentograph on the steady state bedrock profile does not extend infinitely far downstream but instead is damped by diffusion.

### 5.4. Effect of Changing the Peakedness of the Sedimentograph

We now study the effect of the peakedness of the sedimentograph by generalizing the case considered in Figures 9b and 12–14, for which $T$ = 40 years, $r_h$ = 0.25, $L$ = 20 km, and $r_{qh}$ = 3. We use the same values of

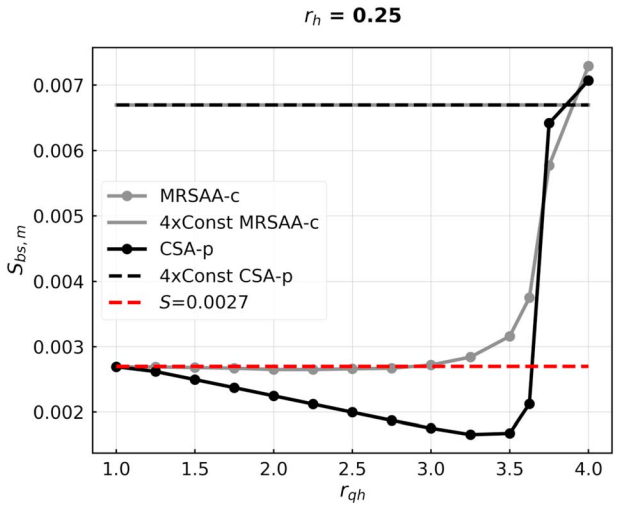


**Figure 16.** Plot of reach-averaged steady state bedrock slope $S_{bs,m}$ versus $r_{qh}$ for $q_{af,m}$ = 0.000834 m$^2$/s (3.5 × 10$^5$ t/year), $T$ = 40 years, $r_h$ = 0.25, and $L$ = 20 km, and with $r_{qh}$ varying from 1 (constant feed rate) to the maximum value 4 ($q_{af,h} = 4 \times q_{af,m}$ for 10 years and 0 for 30 years). Shown in the plot are results from MRSAA-c and CSA-p. Up to the value $r_{qh}$ = 3, MRSAA-c predicts a reach-averaged bedrock slope that differs little from the value for constant feed rate (*MRSAA-c* in legend), as dictated by alluvial diffusive processes. In the case of CSA-p, steady state bedrock slope $S_{bs}$, which is always spatially constant, decreases strongly with increasing sedimentograph amplitude up to $r_{qh}$ = 3 (*CSA-p* in legend). For values of $r_{qh}$ in excess of 3.5, both models predict steeply rising bedrock slope, such that the reach-averaged bedrock slope for the maximum value $r_{qh} = 4$ ($q_{af} = 4 \times 0.000834$ m$^2$/s, or 1.4 × 10$^6$ t/year for 10 years, 0 for 30 years) is not far from the value associated with a constant feed rate equal to $4 \times q_{af,m}$ (= 4 × 0.000834 m$^2$/s) (*4 × Const MRSAA-c* and *4×Const CSA-p* in legend). CSA-p = Capacity Saltation Abrasion, where *p* denotes point formulation; MRSAA-c = corrected Macroroughness Saltation-Abrasion-Alluviation model.

$T$, $r_h$, and $L$ but vary $r_{qh}$. That is, values of the ratio of high feed rate to mean feed rate $r_{qh}$ varying from 1 (constant feed) to the maximum value of 4 (feed rate that is 4 times the mean value for 10 years and 0 for the next 30 years) are considered. Figure 16 shows a plot of reach-averaged bedrock slope at steady state $S_{bs,m}$ versus $r_{qh}$. Results are shown for both CSA-p and MRSAA-c, along with a reference line for constant feed rate ($S$ = 0.0027). It can be seen that for CSA-p, $S_{bs,m}$ declines monotonically below the value for constant feed rate for $r_{qh}$ up to 3. In the case of MRSAA-c, however, $S_{bs,m}$ is very close to the value for constant feed rate up to $r_{qh}$ = 3, again underlining the role of alluvial diffusion. That is, diffusion smears out the sedimentograph, so that the sediment transport rate sufficiently far downstream is roughly constant (Figure 13). For larger values of $r_{qh}$, however, both models predict that $S_{bs,m}$ steeply rises with increasing $r_{qh}$. At $r_{qh}$ = 4, both models predict values of $S_{bs,m}$ that are close to the value 0.0068 corresponding to a constant feed rate at 4 times the mean feed rate of the sedimentograph (abbreviated as $4 \times q_{af,m}$ below). Evidently, a phase change from behavior controlled by the mean feed rate to behavior controlled by the peak feed rate occurs as the sedimentograph becomes very peaky.

Insight concerning this phase change can be obtained from the parameters in Table 3. Here we specifically refer to the values for $r_{qh}$ = 4 and the case of constant feed at rate $4 \times q_{af,m}$. The values of $\overline{p}$ for CSA-p are dramatically different, that is, 0.231 for $r_{qh}$ = 4 but 0.981 for $4 \times q_{af,m}$. The same difference appears for MRSAA-c, in which case the corresponding values for $\overline{p_a}$ are 0.245 and 0.981.

With these differences in mind, how is that the bedrock slope $S_{bs,m}$ is nearly the same (0.0068–0.0073) for the cases $r_{qh}$ = 4 and $4 \times q_{af,m}$? From Table 3, it can be seen that even though the values of $\overline{p}$ and $\overline{p_a}$ are very different for the two cases, the values of $\overline{p(1-p)}$ and $\overline{p_a(1-p_a)}$ are all close to each other (0.017–0.019). As a result, the values of $\overline{q_{ac}p(1-p)}$ (CSA-p) and $\overline{q_{ac}p_a(1-p_a)}$ (MRSAA-c) are sufficiently close between the case $r_{qh}$ = 4 and the $4 \times q_{af,m}$ case so as to give roughly the same steady state slope $S_{bs,m}$.

Figure 17 illustrates the morphodynamics of alluvial cover for the extreme case $r_{qh}$ = 4, for which the sediment feed rate takes the peak value $q_{af,h} = 4 \times 0.000834$ m$^2$/s for 10 years and 0 for the following 30 years. Other parameters are the same as those associated with Figure 9b. Figure 17a shows the spatiotemporal variation of $\eta_a$ over the first 40-year cycle, and Figure 17b shows the temporal variation of $\eta_a$ at $x = 0$, $x = L/2$, and $x = L$ over the same cycle. Note that in this early stage, the cover fraction is zero for substantial periods of time. Notwithstanding, given enough time, the reach attains the macroscopic steady state documented in Figure 16.

### 5.5. Case of Extreme Sedimentograph Peakedness

In all the calculations above, we have used $T$ = 40 years and $r_h$ = 0.25, that is, 10 years of high feed and 30 years of low feed (Figure 3a). We consider a more extreme case in Figures 18 and 19. We retain $T$ = 40 years but reduce $r_h$ to 0.0625, so the feed rate is high for 2.5 years and low for 37.5 years. For this condition, the ratio of high feed rate to mean feed rate $r_{qh}$ varies from 1 to 16. A reduced value of $r_h$ and an increased value of $r_{qh}$ correspond to a more peak sedimentograph. At its highest value, the feed rate is 16 times the mean rate for 2.5 years and 0 for the subsequent 37.5 years. Otherwise, the parameters are the same as those of section 5. We consider two reach lengths: $L$ = 20 and 60 km.

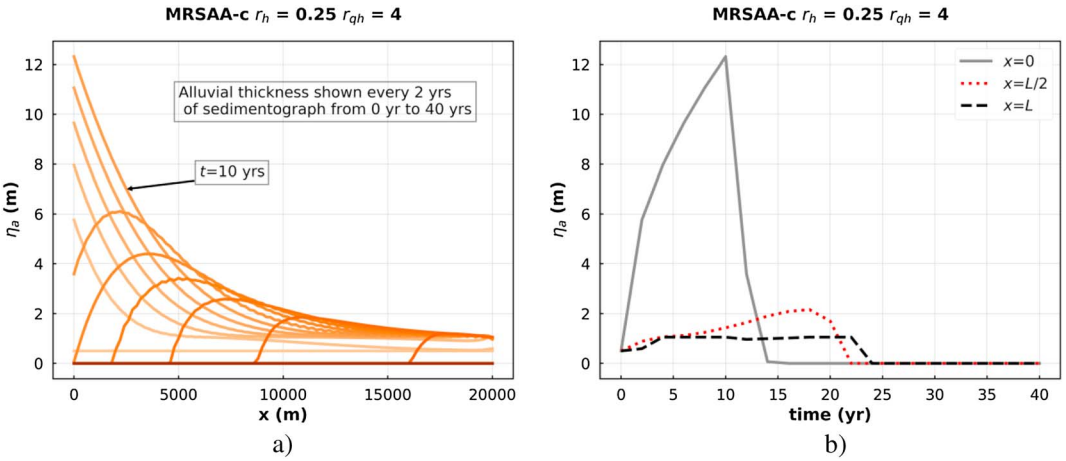


**Figure 17.** Illustration of the early morphodynamics of a case for which $r_{qh} = 4$ (maximum feed rate for 10 years, zero feed rate for 30 years). The other parameters are the same as Figure 9b. (a) The spatiotemporal variation of alluvial cover $\eta_a$ over the first 40 years of the simulation. (b) The corresponding time variation of $\eta_a$ at $x = 0$, $x = L/2$, and $x = L$. MRSAA-c = corrected Macroroughness Saltation-Abrasion-Alluviation model.

Figure 18 shows the results for MRSAA-c for profiles of steady state bedrock slope $S_{bs}$. Three values of $r_{qh}$ are used: 6, 12, and 14. It is again seen that a profile for a short reach plots on top of the profile for a longer reach, just as in Figure 15 for $r_h = 0.25$ and $r_{qh} = 3$. For the case $r_{qh} = 14$, a distinct sedimentograph boundary layer is not evident in Figure 18. The effect of such an extreme sedimentograph propagates to the end of the reach.

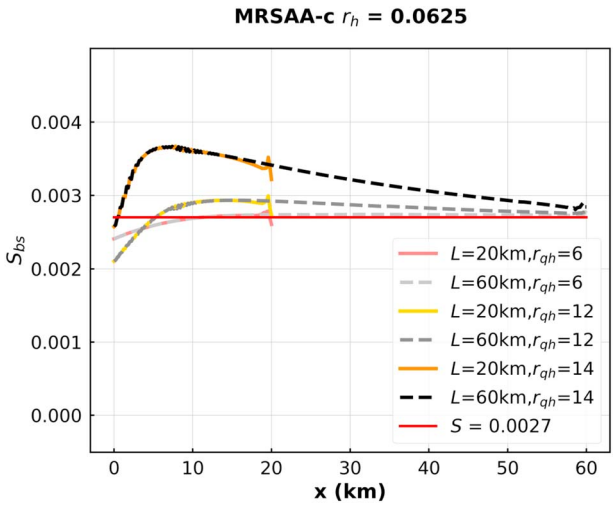


**Figure 18.** The boundary layer and universality properties of the steady state profiles can be further illustrated for the case $r_h = 0.0625$, corresponding to a high feed rate for 2.5 years and a low feed rate for 37.5 years. The plot shows steady state profiles of bedrock slope $S_{bs}$ for the cases $r_{qh} = 6$, 12, and 14 (high feed rate is 6, 12, and 14 times the mean feed rate), with $q_{af,m} = 0.000834$ m$^2$/s ($3.5 \times 10^5$ t/year), $T = 40$ years, and the reach lengths $L = 20$ and 60 km. Also plotted for reference is the case $r_{qh} = 1$ ($S = 0.0027$ in legend). It is seen that for a given value of $r_{qh}$, profiles for different values of reach length $L$ plot on top of each other. A comparison of Figures 15 and 16 reveals that the deviation of $S_{bs}$ from the case of constant feed ($r_{qh} = 1$) increases with peakedness of the sedimentograph (larger $r_{qh}$). The low slope at the upstream end corresponds to the pocket described in Figure 14. MRSAA-c = corrected Macroroughness Saltation-Abrasion-Alluviation model.

Figure 19 shows the variation in alluvial thickness $\eta_a$ over one sedimentograph at steady state, for the case $r_h = 0.0625$ and $r_{qh} = 14$. It is seen that alluvial thickness varies from a low value of 0.1 m to a high value of 31.2 m. We comment more on this repeated massive deposition and flushing in section 6.

### 5.6. Effect of Randomizing the Sedimentograph

Stochasticity of sediment supply events (for example, landslides) can play an important role in both mountain drainage network evolution and incision of the streams therein. This has been modeled in distributed models of landscape evolution by means of a probability density function (PDF) of sediment supply that asymptotically satisfies a power law distribution for large events (Lague, 2010) and also by means of a probabilistic formulation for slope failure based on a slope stability criterion (Egholm et al., 2013). A full exploration of this issue in the context of the present work would require the installation of MRSAA-c into a complete landscape evolution model such as that of Gasparini et al. (2007) or Egholm et al. (2013). Here we consider first calculations using the same values for $q_{af,m} = 0.000834$ m$^2$/s ($3.5 \times 10^5$ t/year), $S_{bi} = 0.004$, and $Cz = 10$ as in section 4. We choose $L = 20$ km and $r_h = 0.0625$ and allow the ratio of high feed rate to mean feed rate $r_{qh}$ to vary randomly in increments of 0.5 between 6 and 12. An example of such a sedimentograph is shown in Figure 4.

Results of the calculations using three realizations of random sequences are shown in Figure 20, where the profile of bedrock slope $S_b$ is shown. There is no precise steady state in the randomized case; instead, we present the results of an 80-year running average,

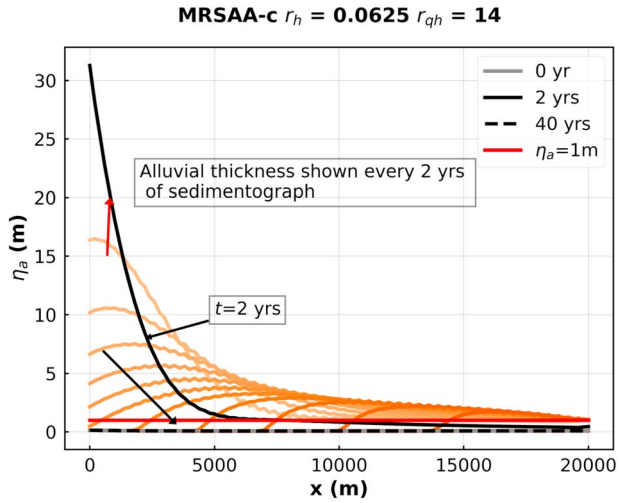


**Figure 19.** Variation of profiles of alluvial thickness $\eta_a$ over one cycle of sedimentograph at steady state for the case $r_h$ = 0.0625 and the ratio of high feed rate to mean feed rate $r_{qh}$ = 14. Thickness varies by as much as 31.2 m at the upstream end, which corresponds to the pocket described in Figure 14. Here $q_{af,m}$ = 0.000834 m$^2$/s (3.5 × 10$^5$ t/year), $T$ = 40 years, and $L$ = 20 km. The red line, red arrow, and black arrow have the same meaning as in Figures 10 and 11. MRSAA-c = corrected Macroroughness Saltation-Abrasion-Alluviation model.

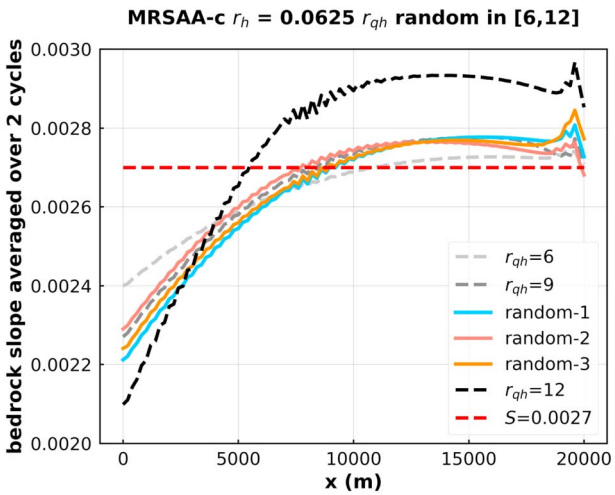


**Figure 20.** Illustration of the effect of randomization of sediment feed on long-term reach-averaged bedrock slope. The lines labeled *random-1*, *random-2*, and *random-3* correspond to three cases for which the ratio of high feed rate to mean feed rate $r_{qh}$ is randomly selected among a uniform distribution of the values [6, 6.5, 7, …, 11.5, 12]. Steady state is somewhat difficult to define in this case; the bedrock slopes correspond to 80-year averages starting from 8,000 years to 8,080 years. Other parameters are $q_{af,m}$ = 0.000834 m$^2$/s (3.5 × 10$^5$ t/year), $T$ = 40 years, $L$ = 20 km, and $r_h$ = 0.0625 (high feed for 2.5 years and low feed for 37.5 years). Also shown are the corresponding curves for bedrock slope at steady state $S_{bs}$ for $r_{qh}$ = 1, 6, 9, and 12. In all of these cases, an effective steady state is reached before 8,000 years. The plot shows that the pocket and the boundary layer effect are preserved even when the input sedimentograph is randomized.

8,000 years after commencement of the run. Also shown for reference in the figure are profiles of $S_{bs}$ for $r_{qh}$ = 6, 9, 12, and 1 (constant feed rate). The profile based on randomized sedimentographs with $r_{qh}$ varying from 6 to 12 is fairly close to the nonrandom profile with $r_{qh}$ = 9. This suggests the absence of strong nonlinear feedbacks in the simplified model presented here.

## 6. Discussion

It can be seen from Figures 1a to 1c that in each case a landslide has caused burial of the stream in deep alluvium. On an event basis, this burial should shut off incision. Yet in the long term, incision can be expected to balance rock uplift. Our work addresses how this can be achieved: the formation of the sedimentograph boundary layer creates a pocket where alluvium is stored but can be evacuated for a sufficient amount of time between landslides to allow long-term incision to balance rock uplift.

Figure 19 shows repeated massive deposition of sediment, followed by nearly complete removal, at the upstream end of the reach. Impulsive aggradation on the order of tens of meters can indeed occur in areas subject to heavy landsliding (Chen & Petley, 2005; Yanites et al., 2010). Two factors, however, must be taken into account in interpreting the results. The first factor is that of debris flows. Landslide deposits of such a thickness are likely to generate debris flows that run down the channel, which are only subsequently reworked by the fluvial flows considered here. The second factor is that of landslide dams (for example, Figure 1a) and their overtopping. The 2008 earthquake in Sichuan, China resulted in the formation of over 200 landslide dams (Fu et al., 2011; Xu et al., 2009). The normal flow model presented here is insufficient to capture the formation and breaching of landslide dams. The minimal formulation for such a case is a treatment with a backwater formulation (e.g., Cui et al., 2006). In order to capture the full morphodynamics, however, treatment with the fully unsteady Saint Venant equations may be necessary. This, notwithstanding, landslide dams typically breach in months to a few years (e.g., Cui et al., 2006; Hancox et al., 2005), validating the use of the normal flow model over the much longer time scales for the adjustment of bedrock elevation.

The model uses a single point source at the upstream end of the reach. In reality, landslides could occur at many locations. We speculate here that (a) there are preferential paths delivering landslide material to a river (for example, gullies or small tributaries) and (b) the confluences of these paths with the river might be prime locations for the formation of bedrock pockets. Verification of this hypothesis may be dependent on the development of new technology, analogous to ground penetrating radar, which can image the alluvial-bedrock interface.

In most of the simulations shown above, the period $T$ of the sedimentograph is held at 40 years with a high feed time rate of either $r_h$ = 0.25 or $r_h$ = 0.0625. The mean sedimentograph feed rate $q_{af,m}$ is 0.000834 m$^2$/s in all cases, the grain size $D$ is 20 mm in all cases, and the flood intermittency $I$ is 0.05 in all cases (as the case of Figure 9b). Here we consider variant cases.

Specifically, we study the effects of varied sedimentograph duration $T$, fraction of time $r_h$ corresponding to high feed rate, alluvial grain size $D$,

and intermittency $I$. We consider three cases with $T = 20$ years, $r_h = 0.5$ (high feed for 10 years), and $r_{qh} = 1$, 1.25, and 1.5 (high feed rate = $1 \times 0.000834$ m$^2$/s, $1.25 \times 0.000834$ m$^2$/s, and $1.5 \times 0.000834$ m$^2$/s), with other parameters held to the same values as in the case described in Figure 9b.

In the case of shortened sedimentograph feed time, the results for macroscopic steady state slope $S = 0.0027$ are the same as the corresponding steady state value 0.0027 shown in Figure 16. That is, shorter $T$ and shorter $T_l$ do not influence the final steady state with the same mean sedimentograph feed rate. Correspondingly keeping all other parameters constant but varying $D$ through 10, 20, and 40 mm, we find reach-averaged bedrock slopes at macroscopic equilibrium of 0.0019, 0.0027, and 0.0045, respectively. Thus, mean bedrock slope at macroscopic equilibrium increases with increasing alluvial grain size. Similarly, we consider the parameters used in Figure 9b but with varying flood intermittency. With the values $I = 0.025$, 0.05, and 0.10, we obtain the reach-averaged bedrock slopes at macroscopic equilibrium of 0.0034, 0.0027, and 0.0024, respectively. This means that the bed slope at macroscopic equilibrium decreases with increasing frequency of flooding.

Here we use the saltation-abrasion model of incision associated with gravel clasts as an example. We do not imply, however, that this is the unique mechanism for bedrock incision. Incision could also be driven by plucking (e.g., Chatanantavet & Parker, 2009; Dubinski & Wohl, 2013), whereby chunks of bedrock are torn from the bed independently of gravel movement, or sandblasting (Lamb et al., 2008), whereby suspended sand can abrade the bed without necessarily maintaining a cover layer. Our model would have to be modified to incorporate these mechanisms; the quoted references provide the basis for doing so.

Relatively few incisional landscape evolution models route alluvium morphodynamically through a river system (e.g., Croissant et al., 2017; Lague, 2010). Our analysis helps underline the importance of doing so. In a model that does not route alluvium morphodynamically (CSA-p), the mean slope of the reach is strongly affected by the peak of the sedimentograph. More specifically, Figure 16 shows that up to some limit, the higher the peak, the lower is the mean slope at macroscopic equilibrium. In a model that does perform this routing (MRSAA-c), the corresponding mean slope is dependent on only the mean, and not the peak, of the sedimentograph, up to a very high peak resulting in phase transition (Figure 16). The reason for this difference is the diffusive behavior of MRSAA-c, as shown in Figure 13.

The precise dynamics of the sedimentograph boundary layer are not elaborated upon in detail here. Suffice it to say that the controlling parameters are the same as those of the hydrograph boundary layer (Wong & Parker, 2006b). Let $\delta$ denotes the thickness (length) of the boundary layer, and recall that length reach is $L$ and sedimentograph period is $T$. Then $\delta/L \sim (T/T_m)^{1/2}$, where $T_m \sim S_b L/q_{af}$ is a scale for morphological response time.

## 7. Conclusions

Here we study the effect of temporally varying sediment supply on bedrock incision, and the associated state in balance with uplift, in mixed bedrock-alluvial rivers. Our work is motivated by the observation that sediment supply in such streams can be highly discontinuous and episodic, especially in geologically young mountain regions subject to earthquakes and intense rainstorms. We vary sediment supply cyclically in time. The starting points for our analysis are two models of bedrock morphodynamics: the CSA model, which does not route alluvium over bedrock, and its extension, the MRSAA model, which does route alluvium. Both models are implemented in deterministic and stochastic frameworks. CSA computes local bedrock incision rate based on local sediment transport rate and areal fraction of alluvial cover. However, it does not include a way to route sediment downstream. Consequently, in our implementation of the model, the sediment transport rate instantaneously equals the feed rate everywhere downstream. We term this implementation CSA-p, where p stands for *point model*. CSA-p characterizes morphodynamic change in terms of advection, as expressed in terms of upstream-migrating incisional features such as knickpoints. MRSAA relates the areal fraction of alluvial cover, and thus the incision rate, to the ratio of alluvial thickness to a characteristic macroroughness of the bedrock itself. It adds an equation for conservation of alluvium, thus characterizing the problem as advective-diffusive. It easily captures spatiotemporal transitions between complete and deep alluviation, when

the bed is protected for a period from incision, to partial alluviation, when the bed can incise. Our results are as follows.

- MRSAA is incorrect in one aspect: it predicts a very small residual incision rate even when the transport rate of alluvium is zero. The formulation presented herein, termed MRSAA-c, corrects this so that the incision rate drops to zero at a very small but nonzero alluvial transport rate.
- The essential difference between CSA-p and MRSAA-c is that the former model does not include the effects of alluvial diffusion, whereas the latter does. The differences between the two models are negligible for constant sediment supply rate but differ in the case of a feed sedimentograph.
- We study numerically the evolution toward a steady state river longitudinal profile for which incision balances a constant uplift rate. We characterize varying sediment supply in terms of a two-step sedimentograph, having a characteristic duration of 40 years and a square signal variation. For one set of numerical runs, the sediment feed rate is given peak values ranging from 1 to 4 times the mean rate for 10 years and is given the corresponding low input rate for 30 years necessary to achieve the specified mean value. In another set allowed to characterize strongly peaked (or flashy) sedimentographs, the period of peak input is 2.5 years, and the period of low input is 37.5 years, with the peak value ranging from 1 to 16 times the mean rate. We find that notable differences can arise between the predictions of CSA-p and MRSAA-c under a sedimentograph.
- In the case of CSA-p, the bedrock slope at steady state is spatially constant, regardless of the sedimentograph. In the case of MRSAA-c, however, the steady state bedrock slope varies downstream, more strongly so as sedimentograph amplitude increases. In the region adjacent to the feed point, the bedrock slope is low, creating a pocket in the bedrock longitudinal profile within which bed elevation (top of bedrock + alluvial thickness) can vary over meters or tens of meters as alluvium cyclically accumulates and is evacuated. Somewhat farther downstream, the bedrock slope is elevated compared to the value prevailing for the case of constant feed rate, but sufficiently far downstream it converges to a constant value.
- The longitudinal profiles of steady state bedrock slope predicted by MRSAA-c display both a boundary layer effect and a universality in profile. Deviations from spatially constant bedrock slope are concentrated in a boundary layer near the feed point, the length of which increases with increasing sedimentograph amplitude. In addition, for otherwise unchanged conditions, bedrock slope values for a 20-km reach plot exactly on top of those for the first 20 km of a 120-km reach.
- For the CSA-p model, the spatially constant bedrock slope at steady state decreases notably with increasing sedimentograph amplitude up to a critical amplitude. For the MRSAA-c model, however, the reach-averaged bedrock slope at steady state remains essentially insensitive to sedimentograph amplitude up to a critical amplitude. This invariance is due to diffusive effects in MRSAA-c; even a high-amplitude sedimentograph is damped downstream due to alluvial diffusion.
- Beyond a critical sedimentograph amplitude, both CSA-p and MRSAA-c exhibit a phase change toward dramatically increased steady state bedrock slope. More specifically, the extremely high reach-averaged bedrock slope realized when sediment is fed at a very high rate for a short time, and no sediment is fed for the rest of the sedimentograph, no longer reflects the slope associated with the mean feed rate. It instead reflects the much steeper value prevailing when the same very high feed rate is held constant in time. This phase transition corresponds to the breakdown of the sedimentograph boundary layer.

The present model, that is, MRSAA-c, is not easily verified in detail based on field data, because the events leading to high-amplitude variation in sediment supply to mountain rivers are difficult to quantify. The real value of the new method is likely to come through its use in a landscape evolution model that resolves individual streams. Gasparini et al. (2007) offer a predecessor in this regard. Two key elements of such a model would be the inclusion of event stochasticity (e.g., Lague, 2010) and width variation (Croissant et al., 2017). The landscape evolution model of Egholm et al. (2013) includes both randomized sediment supply through landslides and a version of CSA-p. Kwang and Parker (2017) have included the formulation presented here, that is, MRSAA-p, into a simplified landscape evolution model that allows the characterization of the effect of short-term spatiotemporally varying sediment cover, including complete evacuation and local complete conversion to alluvial reaches, on the long-term evolution of the landscape itself. The key contribution of the present model to the work of Kwang and Parker (2017) lies in the ability of alluviation to locally turn off incision for substantial periods of time.

## Notation

$B$ channel width (L);
$Cz$ dimensionless Chezy resistance coefficient (1);
$D$ gravel grain size (L);
$E$ incision rate ($LT^{-1}$);
$Fr$ Froude number (1);
$g$ gravitational acceleration ($LT^{-2}$);
$H$ flow depth (L);
$I$ flood intermittency (1);
$L$ reach length (L);
$L_{mr}$ bedrock macroroughness (L);
$p$ alluvial cover fraction, that is, areal fraction of bedrock that is covered with alluvium (averaged over an appropriate window) (1);
$p_a$ adjusted alluvial cover fraction in MRSAA model (1);
$p_l$ lower reference cover fraction (0.05 herein) (1);
$p_h$ upper reference cover fraction (0.95 herein) (1);
$q_a$ volume bedload transport rate per unit width ($L^2\,T^{-1}$);
$q_{ac}$ capacity bedload transport rate per unit width ($L^2\,T^{-1}$);
$q_{af}$ volume bedload feed rate per unit width at upstream ($L^2\,T^{-1}$);
$q_{af,h}$ high-volume bedload feed rate per unit width of sedimentograph ($L^2\,T^{-1}$);
$q_{af,l}$ low-volume bedload feed rate per unit width of sedimentograph ($L^2\,T^{-1}$);
$q_{af,m}$ mean bedload feed rate per unit width of sedimentograph ($L^2\,T^{-1}$);
$Q$ flood discharge ($L^3\,T^{-1}$);
$R$ submerged specific gravity of sediment, $= (\rho_s/\rho) - 1$, where $\rho$ is water density (1);
$r_h$ $= T_h/T$ (1);
$r_l$ $= T_l/T$ (1);
$r_{qh}$ $= q_{bf,h}/q_{bf,m}$ (1);
$r_{ql}$ $= q_{bf,l}/q_{bf,m}$ (1);
$S$ bed slope $= -\partial\eta/\partial x$ (1);
$S_b$ slope of bedrock surface $= -\partial\eta_b/\partial x$ (1);
$S_{bi}$ initial bedrock slope, that is, initial value of $S_b$ (1);
$S_{bs}$ steady state bedrock slope (1);
$S_{bs,m}$ reach-averaged value of $S_{bs}$ (1);
$t$ time (T);
$T$ period of sedimentograph (T);
$T_h$ time duration of high sediment feed of sedimentograph (T);
$T_l$ time duration of low sediment feed of sedimentograph (T);
$U$ flow velocity ($LT^{-1}$);
$x$ streamwise coordinate (L);
$z_l$ elevation associated with cover fraction $p_l$ (L);
$z_h$ elevation associated with cover fraction $p_h$ (L);
$\beta$ bedrock abrasion coefficient ($L^{-1}$);
$\eta$ bed elevation (L);
$\eta_b$ elevation of base of bedrock (L);
$\eta_a$ thickness of alluvial cover (L);
$\lambda$ porosity of alluvial deposit (1);
$\rho_s$ sediment density ($ML^{-3}$);
$\tau^*$ Shields number (1);
$\tau_c^*$ critical Shields number (1);
$\tau$ bed shear stress ($ML^{-1}\,T^{-2}$);
$\upsilon$ rock uplift rate ($LT^{-1}$).
$\varphi_i$ the constant fraction of the alluvial thickness to the macroroughness $L_{mr}$ at $t = 0$ (1).

**Acknowledgments**
The participation of Parker and Stark was made possible in part by a grant from the U.S. National Science Foundation (EAR-1124482). The participation of Parker was also made possible in part by the National Center for Earth-surface Dynamics, a Science and Technology Center funded by the U.S. National Science Foundation (EAR-0120914). This paper is supported by National Natural Science Foundation of China 51569026. The code of MRSAA-c model is available at https://github.com/csdms-contrib/MRSAA. All the data in this paper are shown in the supporting information. John Buffington, Mikaël Attal, and three anonymous reviewers greatly strengthened this paper.

## References

An, C. G., Cui, Y. T., Fu, X. D., & Parker, G. (2017). Gravel-bed river evolution in earthquake-prone regions subject to cycled hydrographs and repeated sediment pulses. *Earth Surface Processes and Landforms*, *42*(14), 2426–2438. https://doi.org/10.1002/esp.4195

An, C. G., Fu, X. D., Wang, G. Q., & Parker, G. (2017). Effect of grain sorting on gravel-bed river evolution subject to cycled hydrographs: Bedload sheets and breakdown of the hydrograph boundary layer. *Journal of Geophysical Research: Earth Surface*, *122*, 1513–1533. https://doi.org/10.1002/2016JF003994

Attal, M. (2017). Linkage between sediment transport and supply in mountain rivers. In D. Tsutsumi, & J. B. Laronne (Eds.), *Gravel-bed rivers, processes and disasters* (chap. 12, pp. 329–353). Oxford, UK: Wiley-Blackwell.

Benda, L., & Dunne, T. (1997). Stochastic forcing of sediment supply to channel networks from landsliding and debris flow. *Water Resources Research*, *33*(12), 2849–2863. https://doi.org/10.1029/97WR02388

Chatanantavet, P., Lajeunesse, E., Parker, G., Malverti, L., & Meunier, P. (2010). Physically based model of downstream fining in bedrock streams with lateral input. *Water Resources Research*, *46*, W02518. https://doi.org/10.1029/2008WR007208

Chatanantavet, P., & Parker, G. (2008). Experimental study of bedrock channel alluviation under varied sediment supply and hydraulic conditions. *Water Resources Research*, *44*, W12446. https://doi.org/10.1029/2007WR006581

Chatanantavet, P., & Parker, G. (2009). Physically based modeling of bedrock incision by abrasion, plucking, and macroabrasion. *Journal of Geophysical Research*, *114*, F04018. https://doi.org/10.1029/2008JF001044

Chen, H., & Petley, D. N. (2005). The impact of landslides and debris flows triggered by typhoon Mindulle in Taiwan. *Quarterly Journal of Engineering Geology & Hydrogeology*, *38*(3), 301–304. https://doi.org/10.1144/1470-9236/04-077

Chou, H. T., Lee, C. F., & Lo, C. M. (2017). The formation and evolution of a coastal alluvial fan in eastern Taiwan caused by rainfall-induced landslides. *Landslides*, *14*(1), 109–122. https://doi.org/10.1007/s10346-016-0678-6

Croissant, T., Lague, D., Steer, P., & Davy, P. (2017). Rapid post-seismic landslide evacuation boosted by dynamic river width. *Nature Geoscience*, *10*(9), 680–684. https://doi.org/10.1038/ngeo3005

Cui, Y., Parker, G., Braudrick, C., Dietrich, W. E., & Cluer, B. (2006). Dam Removal Express Assessment Models (DREAM). Part 1: Model development and validation. *Journal of Hydraulic Research*, *44*(3), 291–307. https://doi.org/10.1080/00221686.2006.9521683

Cui, Y., Parker, G., Lisle, T., Gott, J., Hansler, M., Pizzuto, J. E., et al. (2003). Sediment pulses in mountain rivers. Part 1. Experiments. *Water Resources Research*, *39*(9), 1239. https://doi.org/10.1029/2002WR001803

Cui, Y., Parker, G., Pizzuto, J. E., & Lisle, T. E. (2003). Sediment pulses in mountain rivers. Part 2. Comparison between experiments and numerical predictions. *Water Resources Research*, *39*(9), 1240. https://doi.org/10.1029/2002WR001805

Dadson, S. J., Hovius, N., Chen, H., Brian Dade, W., Hsieh, M. L., Willett, S. D., et al. (2003). Links between erosion, runoff variability and seismicity in the Taiwan orogeny. *Nature*, *426*(6967), 648–651. https://doi.org/10.1038/nature02150

DiBiase, R. A., & Whipple, K. X. (2011). The influence of erosion thresholds and runoff variability on the relationships among topography, climate, and erosion rate. *Journal of Geophysical Research*, *116*, F04036. https://doi.org/10.1029/2011JF002095

Dubinski, M. I., & Wohl, E. (2013). Relationships between block quarrying, bed shear stress, and stream power: A physical model of block quarrying of a jointed bedrock channel. *Geomorphology*, *180-181*, 66–81. https://doi.org/10.1016/j.geomorph.2012.09.007

Egholm, D. L., Knudsen, M. F., & Sandiford, M. (2013). Lifespan of mountain ranges scaled by feedbacks between landsliding and erosion by rivers. *Nature*, *498*(7455), 475–478. https://doi.org/10.1038/nature12218

Ferguson, R. I., Church, M., Rennie, C. D., & Venditti, J. G. (2015). Reconstructing a sediment pulse: Modeling the effect of placer mining on Fraser River, Canada. *Journal of Geophysical Research: Earth Surface*, *120*, 1436–1454. https://doi.org/10.1002/2015JF003491

Fernandez Luque, R., & Van Beek, R. (1976). Erosion and transport of bed-load sediment. *Journal of Hydraulic Research*, *14*(2), 127–144. https://doi.org/10.1080/00221687609499677

Fu, X. D., Liu, F., Wang, G. Q., Xu, W. J., & Zhang, J. (2011). Necessity of integrated methodology for hazard mitigation of quake lakes: Case study of the Wenchuan earthquake, China. *Frontiers of Architecture and Civil Engineering in China*, *5*(1), 1–10. https://doi.org/10.1007/s11709-011-0099-5

Gasparini, N. M., Whipple, K. X., & Bras, R. L. (2007). Predictions of steady state and transient landscape morphology using sediment-flux-dependent river incision models. *Journal of Geophysical Research*, *112*, F03S09. https://doi.org/10.1029/2006JF000567

Golly, A., Turowski, J. M., Badoux, A., & Hovius, N. (2017). Controls and feedbacks in the coupling of mountain channels and hillslopes. *Geology*, *45*(4), 307–310. https://doi.org/10.1130/G38831.1

Hancox, G. T., McSaveney, M. J., Manville, V. R., & Davies, T. R. (2005). The October 1999 Mt. Adams rock avalanche and subsequent landslide dam-break flood and effects in Poerua River, Westland, New Zealand. *New Zealand Journal of Geology and Geophysics*, *48*(4), 683–705. https://doi.org/10.1080/00288306.2005.9515141

Hovius, N., Stark, C. P., Chu, H. T., Hao-Tsu, C., & Lin, J. C. (2000). Supply and removal of sediment in a landslide-dominated mountain belt: Central range, Taiwan. *Journal of Geology*, *108*(1), 73–89. https://doi.org/10.1086/314387

Huang, M. Y. F., & Montgomery, D. R. (2012). Fluvial response to rapid episodic erosion by earthquake and typhoons, Tachia River, central Taiwan. *Geomorphology*, *175-176*, 126–138. https://doi.org/10.1016/j.geomorph.2012.07.004

Kwang, J. S., & Parker, G. (2017). Landscape evolution using a sediment flux-dependent bedrock incision model incorporating bedrock macro-roughness. Abstract EP43A-0937, presented at *2017* AGU Fall Meeting, New Orleans, LA, 11–15.

Lague, D. (2010). Reduction of long-term bedrock incision efficiency by short-term alluvial cover intermittency. *Journal of Geophysical Research*, *115*, F02011. https://doi.org/10.1029/2008JF001210

Lague, D., Hovius, N., & Davy, P. (2005). Discharge, discharge variability, and the bedrock channel profile. *Journal of Geophysical Research*, *110*, F04006. https://doi.org/10.1029/2004JF000259

Lamb, M. P., Dietrich, W. E., & Sklar, L. S. (2008). A model for fluvial bedrock incision by impacting suspended and bed load sediment. *Journal of Geophysical Research*, *113*, F03025. https://doi.org/10.1029/2007JF000915

Larsen, J. I., Montgomery, D. R., & Korup, O. (2010). Landslide erosion controlled by hillslope material. *Nature Geoscience*, *3*(4), 247–251. https://doi.org/10.1038/NGEO776

Lisle, T. E., Cui, Y., Parker, G., Pizzuto, J. E., & Dodd, A. M. (2001). The dominance of dispersion in the evolution of bed material waves in gravel-bed rivers. *Earth Surface Processes and Landforms*, *26*(13), 1409–1420. https://doi.org/10.1002/esp.300

Lisle, T. E., Pizzuto, J. E., Ikeda, H., Iseya, F., & Kodama, Y. (1997). Evolution of a sediment wave in an experimental channel. *Water Resources Research*, *33*(8), 1971–1981. https://doi.org/10.1029/97WR01180

Marc, O., Hovius, N., Meunier, P., Gorum, T., & Uchida, T. (2016). A seismologically consistent expression for the total area and volume of earthquake-triggered landsliding. *Journal of Geophysical Research: Earth Surface*, *121*, 640–663. https://doi.org/10.1002/2015JF003732

Meyer-Peter, E., & Müller, R. (1948). Formulas for bed-load transport. *Proceedings of the 2nd Meeting of the International Association for Hydraulic Structures Research*, 39-64.

Parker, G. (1991a). Selective sorting and abrasion of river gravel: Applications. *Journal of Hydraulic Engineering*, *117*(2), 150–171. https://doi.org/10.1061/(ASCE)0733-9429(1991)117:2(150)

Parker, G. (1991b). Selective sorting and abrasion of river gravel: Theory. *Journal of Hydraulic Engineering*, *117*(2), 131–147. https://doi.org/10.1061/(ASCE)0733-9429(1991)117:2(131)

Parker, G. (2004). 1-D sediment transport morphodynamics with applications to rivers and turbidity currents. Retrieved from http://vtchl.uiuc.edu/people/parkerg/

Parker, G., Hassan, M., & Wilcock, P. R. (2007). Adjustment of the bed surface size distribution of gravel-bed rivers in response to cycled hydrographs, gravel-bed rivers VI: From process understanding to river restoration, chapter 10, Habersack, H. Piégay, H., Rinaldi, M., editors. *Developments in Earth Surface Processes*, *11*, 241–285. https://doi.org/10.1016/S0928-2025(07)11127-5

Sklar, L. S., & Dietrich, W. E. (2004). A mechanistic model for river incision into bedrock by saltating bed load. *Water Resources Research*, *40*, W06301. https://doi.org/10.1029/2003WR002496

Sklar, L. S., & Dietrich, W. E. (2006). The role of sediment in controlling bedrock channel slope: Implications of the saltation-abrasion incision model. *Geomorphology*, *82*(1-2), 58–83. https://doi.org/10.1016/j.geomorph.2005.08.019

Sklar, L. S., Fadde, J., Venditti, J. G., Nelson, P., Wydzga, M. A., Cui, Y., & Dietrich, W. E. (2009). Translation and dispersion of sediment pulses in flume experiments simulating gravel augmentation below dams. *Water Resources Research*, *45*, W08439. https://doi.org/10.1029/2008WR007346

Venditti, J. G., Dietrich, W. E., Nelson, P. A., Wydzga, M. A., Fadde, J., & Sklar, L. (2010). Effect of sediment pulse grain size on sediment transport rates and bed mobility in gravel bed rivers. *Journal of Geophysical Research*, *115*, F03039. https://doi.org/10.1029/2009JF00141

Whipple, K. X. (2004). Bedrock rivers and the geomorphology of active orogens. *Annual Review of Earth and Planetary Sciences*, *32*, 151–185. https://doi.org/10.1146/annurev.earth.32.101802.120356

Wong, M., & Parker, G. (2006a). Reanalysis and correction of bed-load relation of Meyer-Peter and Müller using their own database. *Journal of Hydraulic Engineering*, *132*(11), 1159–1168. https://doi.org/10.1061/(ASCE)0733-9429(2006)132:11(1159)

Wong, M., & Parker, G. (2006b). One-dimensional modeling of bed evolution in a gravel-bed river subject to a cycled hydrograph. *Journal of Geophysical Research*, 111, F03018. https://doi.org/10.1029/2006JF000478

Xu, Q., Fan, X. M., Huang, R. Q., & Van Westen, C. (2009). Landslide dams triggered by the Wenchuan earthquake, Sichuan Province, south west China. *Bulletin of Engineering Geology and the Environment*, *68*(3), 373–386. https://doi.org/10.1007/s10064-009-0214-1

Yanites, B. J., Tucker, G. E., Mueller, K. J., & Chen, Y. G. (2010). How rivers react to large earthquakes: Evidence from central Taiwan. *Geology*, *38*(7), 639–642. https://doi.org/10.1130/G30883.1

Zhang, L., Fu, X. D., Stark, C. P., Férnandez-Arrieta, R., & Parker, G. (2013). *Modeling of incision of bedrock rivers subject to temporally varying sediment supply* (p. 11). Beijing: Proceedings of 2013 IAHR Congress, Tsinghua University Press.

Zhang, L., Parker, G., Stark, C. P., Inoue, T., Viparelli, E., Fu, X. D., & Izumi, N. (2015). Macro-roughness model of bedrock-alluvial river morphodynamics. *Earth Surface Dynamics*, *3*(1), 113–138. https://doi.org/10.5194/esurf-3-113-2015